We are IntechOpen, the world's leading publisher of Open Access books Built by scientists, for scientists

6,900
Open access books available

186,000
International authors and editors

200M
Downloads

Our authors are among the

154
Countries delivered to

TOP 1%
most cited scientists

12.2%
Contributors from top 500 universities

CLARIVATE ANALYTICS
BOOK CITATION INDEX
INDEXED

WEB OF SCIENCE™

Selection of our books indexed in the Book Citation Index
in Web of Science™ Core Collection (BKCI)

Interested in publishing with us?
Contact book.department@intechopen.com

4

Fatigue Cracking Behaviors and Influence Factors of Cast Magnesium Alloys

Xi-Shu Wang

Department of Engineering Mechanics, School of Aerospace, AML,
Tsinghua University, Beijing,
China

1. Introduction

Accurate prediction of fatigue performance and life is a key issue in the design and applications of the high strength-to-weight ratio of many contemporary magnesium alloys, which are suitable for ultimate weight reduction purposes in automotive and aircraft components. For example, the ever increasing demands for higher efficiency and light weight typical cases of power generation, aerospace and automotive industries call the maximum exploitation of the material's properties. The combination of low density (about 1.74 g/cm³), high specific strength and excellent castability qualifies magnesium alloys as ideal materials for the lightweight constructions [1]. Thus, purely empirical models that heavily rely on larger safety factors are of limited uses. It is now widely recognized that fatigue damage models that are closely related to the microstructural features to provide a more reliable basis for a life prediction, provided that the relevant microstructural damage mechanisms are accurately accounted for. Therefore, there are increasing interests in the fatigue tests combined with the high-resolution microscopic techniques, environmental influencing factors, and especially in understanding their fatigue crack initiation and propagation behaviors with process rationalization [2-4]. Subsequently experimental observations on cast magnesium alloys have accumulatively revealed that the dendrite cell size, pores, secondary phase particles, persistent slip bands and twinning in the dendrite cells considerably affect on the fatigue durability and fatigue cracking behavior or crack growth mechanism of dendritic magnesium alloys [5-8]. The quantitative estimation of small fatigue crack growth rate of cast magnesium alloys is whether simply and effectively to assist the reversed design of cast magnesium alloys or ceaselessly to improve the strength and toughness of cast magnesium alloys. At the same time, it is necessary how to understand that these microstructural features of cast magnesium alloys play role in the fatigue cracking behavior or that the microstructural evolution reacts to the applied loadings. However, it is difficult to use conventional alloying techniques to improve some of their properties, e.g. elastic modulus, elastic-plastic deforming property and the different thermal expansion between phases during the shrinking at the high elevated temperatures. Under these conditions the elastic, and the possible plastic, properties of the secondary phase will influence the mechanical response during an applied loading since the interface of secondary phase will transmit stresses from the matrix around the secondary phase when the interface both the matrix and secondary phase has a compatible strain field. If the elastic

modulus or elastic-plastic property of the secondary phase is larger than that of the surrounding matrix in the secondary phase will take up a larger load than the matrix next to the secondary phase so that the stresses are reduced in the vicinity of the secondary phase. On the other hand, the modulus of elasticity of the secondary phase is smaller that that of the matrix, the secondary phase will take up a smaller load than the matrix next to the secondary phase so that the stresses are increased in the vicinity of the secondary phase. From the above analysis it is obvious that the secondary phase with different thermal expansion properties or elastic properties compares to the matrix will behave differently with respect to crack initiation and early growth during fatigue loading. Therefore, one must resort to fiber/ particle reinforcement in order to reduce the difference of thermal expansion properties or elastic properties between the secondary phase and the matrix. The solubility of alloying elements in magnesium alloy is limited, which restricts the possibility of improving the mechanical properties and chemical behavior of this material. The crystal structure of magnesium is hexagonal which limits its inherent ductility. The only alloying element, which causes a useful phase change to bcc, in this respect, is lithium. The property profiles demanded by automobile and other large-scale potential users of magnesium alloys have revealed the need for alloy development. A direct transfer of high performance aircraft alloys is not possible on economic grounds and the property profile does not coincide. Ebert et al. [1] previously indicated that there are four development trends based on their main requirements, which are as following respectively: First trend of specific strength is Mg-Al-Mn, Mg-Al-Zn, Mg-Zn-Cu, Mg-Al-Ca (-Re), Mg-Li-X. Second trend of good ductility is Mg-Si, Mg-Al-Ca (-re), Mg-Li-X. Third trend of good creep resistance is Mg-Al-Re, Mg-Al-Ca-X, Mg-Ag-Re-Zr, Mg-Y-Re-Zr, and Mg-Sc-X-Y. And the final trend of good wear, creep, thermal expansion is fibre/ particle reinforced Mg-MMC's. Therefore, the mechanical properties and microstructure of magnesium alloys can be improved by above mentioned development trends [1,9-11]. No matter what development trends in the alloying processes of this material, some microstructural defects are impossibly to be avoided. And, the effects of these microstructural defects on the cracking behavior, the interactions on the microstructural defects and differential phases with different elastic or thermal expansion properties occur mainly in the ranges of meso/ micro scales; therefore, the investigations have to localize in the techniques with high-resolution microscope, especially *in-situ* measurements.

Dating back to the seventies of the last century, the potential of *in-situ* fatigue studies conducted in a scanning electron microscope (SEM) has been realized as SEMs combine the servo-hydraulic loading (provided thermal loading, humid environment etc.) testing system. Since that time, numerous studies have demonstrated that *in-situ* fatigue in the SEM device is an effective tool for the investigation of microstructural effects on the development of slip features [12,13], on crack initiation [2,5,14-19], for the analysis of the mechanisms of crack growth [14-17,20,21], for the quantitative determination of small crack growth rates [14-18,22], crack tip opening displacements [16,23-25], for the examination of interactions between fatigue crack growth and microstructure [15,16,26-28], for the effects of vacuum, high temperature, water vapor environments, notch and pores alignment etc. [6,15,16,29-31]. For example, the majority limitation of most studies were imposed by the fact that the experiments had to be conducted at room temperature (RT) in a high-vacuum, whereas most components typically operate in a gaseous environment, which can simultaneously be combined with the high-temperature conditions and after prior-corrosion magnesium alloys. This is because the magnesium alloys are easily corroded and to have the low creep

resistance. With the advent of environmental scanning electron microscopes (ESEM), the situation has changed considerably. Today's ESEMs typically allow for imaging in various gaseous environments at a pressure up to about 20-30 Torr, and thus, high-resolution data may be obtained under the conditions relevant to those of actual components. Most procedures required for *in-situ* fatigue testing conducted at RT in an ESEM are not much different from those required for tests in high vacuum. Environmental *in-situ* fatigue testing at elevated temperatures and in corrosion conditions, especially in micro/ meso scales, is still in its beginning, and it is hoped that the current study will stimulate a further research in this area, which includes to the multi-scales and multi-dimensions fracture/ fatigue damage mechanics in the reversed design of magnesium alloys with some processing defects.

Following discussions and analyses about the fatigue cracking behaviors and influencing factors of typical cast magnesium alloys are the main aims of this chapter. These involve the considerations of materials science, engineering mechanics and experimental technology at the microstructural level including to the microstructural defects. Principles of these sciences and technology are utilized for a design of microstructures having superior fracture/ failure resistance. The fatigue micro crack initiation and propagation behaviors are especially useful the design against fracture, in providing the improving the approach about the mechanical properties of cast magnesium alloys. The design philosophy inherent to fracture mechanics is that the operating stress must be less than the magnesium alloys' critical fracture stress. The critical stress may be much less in "real" engineering structures than in "flaw-free" magnesium alloy as a result of notches, cracks and pores of macroscopic dimensions that are present to one degree or another in all structural parts. Therefore, the room temperature tests conducted on the cast magnesium alloys are addressed first, as these demonstrate that substantial environmental effects on the fatigue damage evolution can be observed in certain materials even at room temperature. The second part of the chapter focuses on high-temperatures *in-situ* testing, and the provided examples are from recent fatigue tests on the results of fatigue cracking behavior and influencing factors for the typical cast magnesium alloys, which involve the effects of spacing and alignment with two pores on the fatigue crack initiation and propagation behaviors etc.

2. Phenomenological descriptions of typical cast magnesium alloys

2.1 Microstructural characteristics

Scanning electron micrographs at the lower and higher magnifications of typical cast magnesium alloys, such as AZ91D, AZ91, AM60, AM60B, AM50 and additions some mischmetals into these magnesium alloys, were shown in as following Figures. In these SEM images, we see clearly the mainly microstructural components of primary α-Mg cells and β-$Mg_{17}Al_{12}$ phase as shown in Figs. 1A-1E. With increasing of aluminum content, the distribution density of β-$Mg_{17}Al_{12}$ phase becomes larger and larger. As the typical cast AM50 alloy, the microstructural components should consist of the following:

1. Hexagonal α-Mg cells having a linear intercept average size of about 20 μm. However, larger α-Mg cells with an average size of about 50 μm appear in groups within isolated nodules (Figs. 1E). The microstructure of other cast magnesium alloys such as AM60, AZ91, has a similar to that of AM50. The obvious difference of their microstructures is at the size and distribution of α-Mg phase or in the geometrical shape of β-$Mg_{17}Al_{12}$ phase. For example, microstructural morphology of AM60 or AZ91 alloy consists also of α-Mg matrix and secondary phase of β-$Mg_{17}Al_{12}$ or β-$Mg_{17}Al_{12}X$ (X denotes another

element) along grain boundaries as shown in Figs. 1B and 1C, especially in thick section with lower cooling rate.

2.   In these microstructures, there is a little other Mn rich phase inclusion juxtaposed of two particles (as shown in Figs. 1D). As illustrated result in Figs. 1D, this small white particle on the secondary phase represents a distinct phase in a polygonal shape more enriched in Mn and centered on an oval grey precipitate. The polygonal particle is reminiscent of the hexagonal crystal structured Al_8Mn_5 phase reported by Wang et al. in their transmission electron microscopy (TEM) analysis [32]. From the electron probe microanalysis mapping, this phase still contains Mn element but with more enrichment in Al element and a maximum localization of Si element. It may correspond then to an agglomeration of Al_6Mn or/ and AlMnSi phase reported in Refs [33] and [34], respectively. I agree much more that the aforementioned superposition of Mn-rich particles is referred to as Mn-rich inclusion [4].

(A) AM50   (B) AM60   (C) AZ91

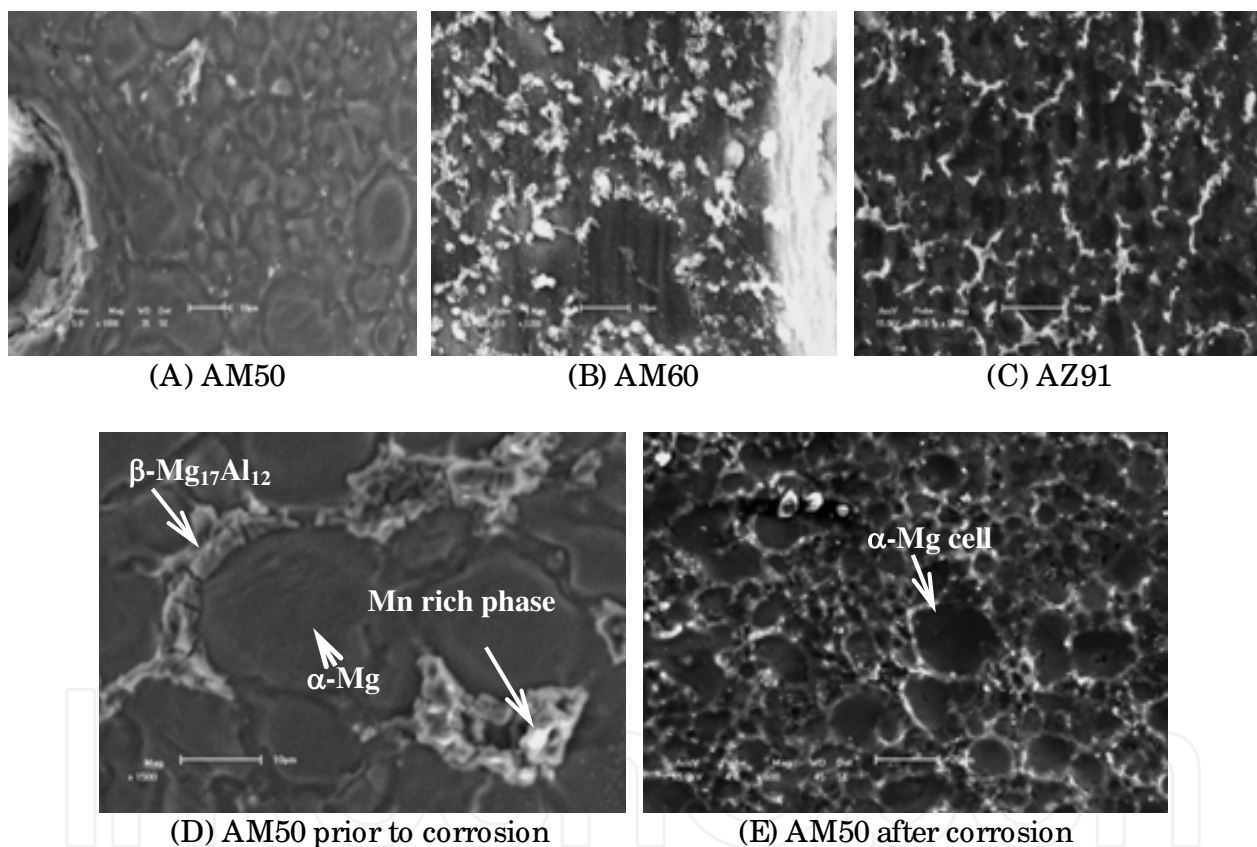(D) AM50 prior to corrosion   (E) AM50 after corrosion

Fig. 1. Typical microstructure of cast magnesium alloys

3.   In addition, the shrinkage pores or other casting defects are also the microstructural feature of cast magnesium alloys as shown in Figs. 2. The shrinkage pores or casting defects are caused by the different deformation rates because there are different thermal expansions and elastic properties between the two phases. These defects of shrinkage clusters located disjointedly in the interdendritic regions. These pores cause the hydrogen penetration into the dendritic structure during solidification, in which the surface of pores occurs easily in the significant plastic striations in micro scale under the applied loading [4].

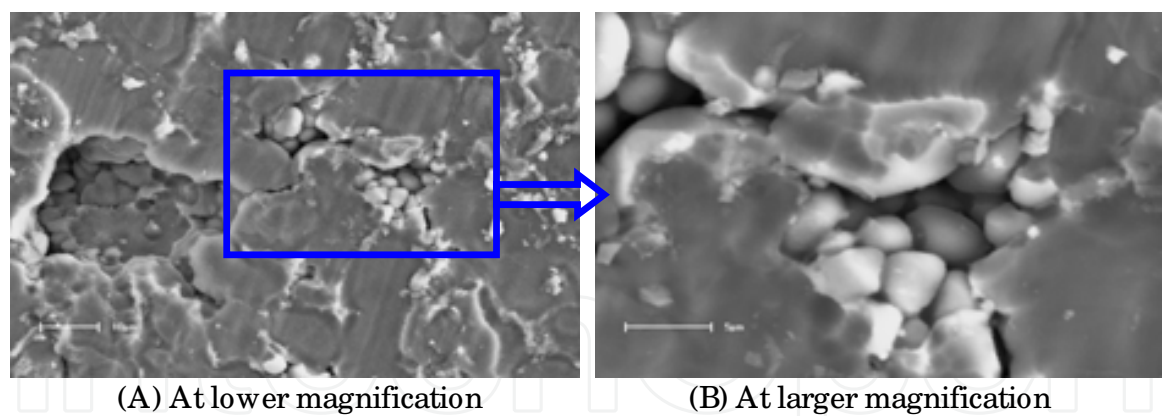(A) At lower magnification (B) At larger magnification

Fig. 2. Typical microstructural defect of cast AM50 alloy

4. The microstructure of typical cast AM50 alloy is present in the brittle eutectic phase (β-$Mg_{17}Al_{12}$) that its micro-hardness is about 88.34 MPa, and is present the softer matrix of primary phase (α-Mg) that its micro-hardness is about 66.86 MPa [15]. As the existent difference of micro-hardness between the two phases, the interface of two phases occurs easily in the deformation mismatch under the applied loading [4,6,10,14-17]. It is thus clear that a pore which is debonded from the matrix will act as a preferential site for crack initiation and crack early growth. The only significant difference between a surface and an internal pore/ debonded β-$Mg_{17}Al_{12}$ is that the former will show more rapid crack growth once the crack has circumvented around the pore/ debonded β-$Mg_{17}Al_{12}$.
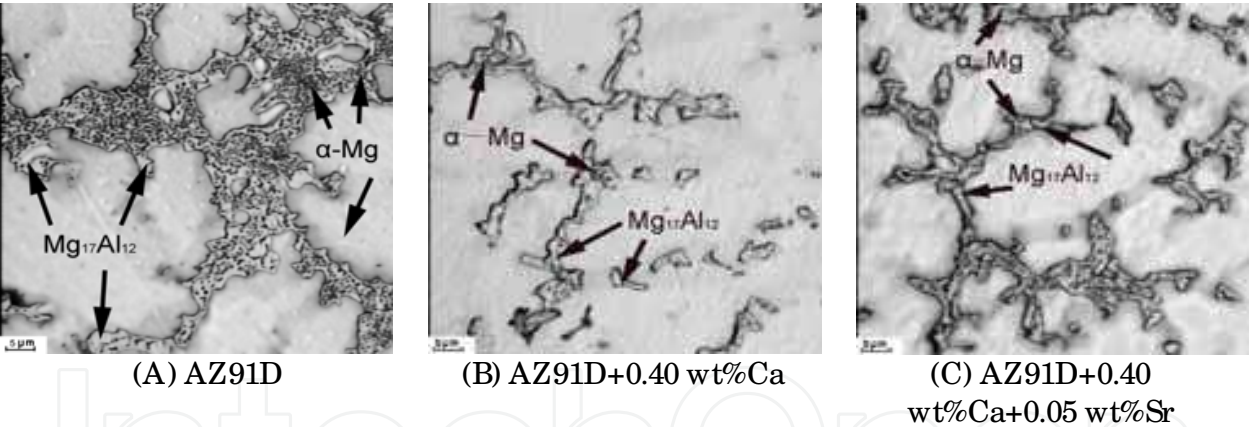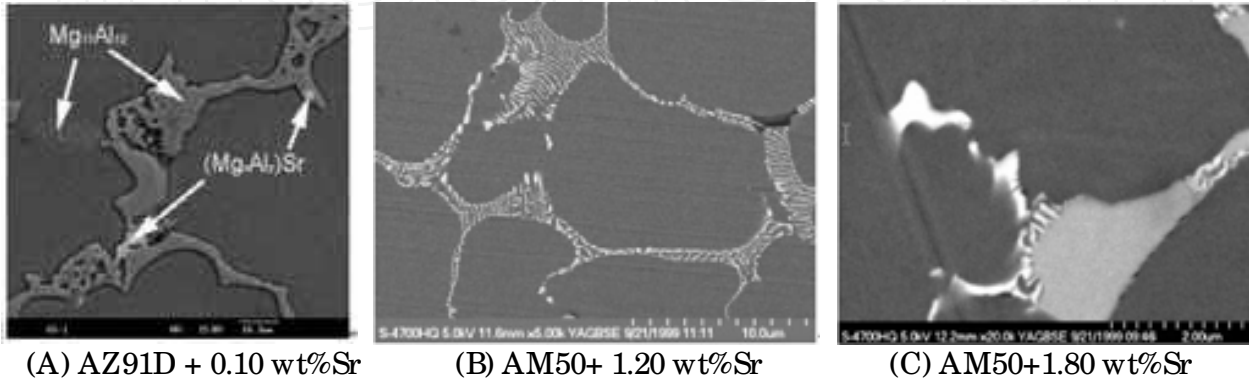

(A) AZ91D (B) AZ91D+0.40 wt%Ca (C) AZ91D+0.40 wt%Ca+0.05 wt%Sr

Fig. 3. Refinement microstructure of cast magnesium alloys with addition of Ca/ Sr

(A) AZ91D + 0.10 wt%Sr (B) AM50+ 1.20 wt%Sr (C) AM50+1.80 wt%Sr

Figs. 4. (Mg_xAl_y)Sr phase distribution of cast magnesium alloys with addition of Sr

5. The rare earths (REs) or Ca etc. have been used in magnesium alloys for many years, whereas the alloys of Mg-Al-RE/ Ca/ Sr system have been developed in the recent decade [35,36]. For example, the refinement influence of the separated and composite addition of Ca and Sr is showed in Figs. 3. We can see that the microstructural features of cast magnesium alloys after refinement influence based on the addition some elements into the matrix. One of many influencing factors is that the β-phase becomes more and more slender when the addition of 0.4 wt%Ca into AZ91D was carried out as shown in Figs. 3A-3B. And other phase such as $(Mg_xAl_y)Sr$ located mainly on the β-$Mg_{17}Al_{12}$ phase thus it can classify as the secondary phase as shown in Figs. 4. Through the addition RE or Ca/ Sr into the Mg alloys, formed the α-Mg grain boundaries can cause the interface to become a more steady than that prior to addition. The behavior of addition REs or Ca/ Sr can improve the mechanical, corrode and hot-crack resistance properties, especially the mechanical property of cast magnesium alloys at high temperatures [9-11,37,38].

2.2 Mechanical properties

As above mentioned, some microstructural features, such as a dendrite, interdendritic pore, shrinkage pores, and secondary phase particles, are the important factors to affect on the mechanical properties. On the other hand, the boundary strengthening by addition RE or Ca/ Sr elements can improve the mechanical properties of cast magnesium alloys. Therefore, the main chemical compositions and mechanical properties of typical cast magnesium alloys used the fatigue cracking tests in this chapter were listed in Table 1. And in these typical cases, the effects of addition Ca/ Sr into AZ91D alloy on the mechanical properties were listed as shown in Table 2.

Alloys	Al	Mn	Zn	Si	Yield stress $\sigma_{0.2}$ (MPa)	Tensile stress σ_b (MPa)	Elongation $\delta\%$
AM50	4.5-5.3	0.2-0.5	<0.2	1.2	135	200	9-10
AM60	5.99	0.2	0.22	1.2	160	210	4-7
AM60B	5.5-6.5	0.2-0.6	0.25	1.0	150	240	10-12
AZ91	8.2-9.5	0.15-0.4	0.92	0.05	180	250	3.0-3.5
AZ91D	8.3-9.7	0.15-0.5	0.35-1.0	0.10	72	160	1.7-1.9

Table 1. Main chemical compositions and mechanical properties of typical cast Mg alloys

In Table 2, it is clearly seen that the yield stress of AZ91D increase slightly but the tensile stress and elongation decreases slightly with the increasing addition Ca amount into the cast AZ91D at RT. The mechanical properties improved well under the slightly composite addition of Ca and Sr. It is because that ductility parameter as mechanical properties of cast magnesium alloy is determined by the number of operative slip systems. Mg being hexagonal slips at room temperature on the base plane (0001) <1120> and secondary slip on vertical face planes (1010) in the <1120> direction. This limits ductility at the lower temperatures. At elevated temperatures slip also occurs in the $< 11\hat{2}0 >$ direction on the

$(10\bar{1}1)$ pyramidal planes. This behavior is influenced by an alloying, but as long as the structure remains hexagonal the effects based on Mg-Si and Mg-Al-Ca-(RE) and Mg-Li-X,

Composition (Wt %)	RT tensile			150 °C tensile		
	Yield stress $\sigma_{0.2}$ (MPa)	Tensile stress σ_b (MPa)	Elongation $\delta\%$	Yield stress $\sigma_{0.2}$ (MPa)	Tensile stress σ_b (MPa)	Elongation $\delta\%$
AZ91D	72	160	1.67	58	105	4.8
AZ91D-0.40Ca	83	145	1.30	70	97	3.0
AZ91D-0.60Ca	84	143	1.30	-	-	-
AZ91D-1.00Ca	86	138	0.99	-	-	-
AZ91D-0.40Ca-0.05Sr	80	152	1.49	68	112	3.7
AZ91D-0.40Ca-0.10Sr	76	150	1.51	65	108	3.9

Table 2. Mechanical properties of the typical cast Mg alloys with an addition Ca/ Sr

which offer the possibility of having a phase mixture of bcc and hcp phase, there has been punch work into the development of fine grain material. One such technique, which has been proved successful in the case of aluminum and copper based alloys and steels, is spray forming fine grain material [1]. However, the composite addition a little Ca/ Sr into AZ91D caused the yield stress of cast magnesium alloy much more to be improved than that single addition Ca into AZ91D. Another importance mechanical property of cast magnesium alloy is the tensile behavior (including to the tensile strength and ductile properties of material), which comes from the typical tensile tests about the cast AM60B and AZ91D at room and elevated temperatures were carried out with the smooth specimens. The tensile behaviors by these tensile curves of cast magnesium alloys as shown in Figs. 5 are better than that by Table 2. In the Figs. 5A, the effect of the elevated temperature (which is over than 150 °C or 423K) on the strength of cast AM60B can be not ignored but the effect of the elevated temperature on the strength of cast AM60B+0.05wt%Sr is not obvious as shown in Figs. 5A. This is because the addition slight Sr into AM60B caused the α-Mg grain coarsening [38]. The coarsening grain will influence the tensile properties of AM60B compared with the results before and after addition of slight Sr amount at the RT condition but with a slight influence on the tensile properties at the elevated temperature. However, for the cast AZ91D, before and after addition 0.05-0.10 wt%Sr, you can clearly see that the effect of elevated temperature and addition a slight Sr amount on the strength and ductile properties can be also not ignored as shown in Figs. 5B. But, there is still not clear issue on the influence mechanism of cast magnesium alloys nowadays during these additional processes and at the critical transferred temperature of cast magnesium alloys. Many researchers thought that mischmetal has grain refinement effect on AZ31, AZ61 and AZ91 alloys, and put forward the grain refinement mechanism as follows. During the solidification process, mischmetal enriched in front of solid/ liquid interface, and gave rise to growth of α-Mg dendrites was suppressed and resulted in grain refinement. But no micrographs were given showing grain structures before and after mischmetal addition into AZ31, AZ61 and AZ91

alloys [38]. Another literature mentioned that small addition of pure cerium and mischmetal consisting of La and Ce led to considerable grain coarsening in AM50 alloy, and grain structures before and after mischmetal addition were shown, however, there was no explanation about the grain coarsening mechanism [39]. Although the experimental conditions in each researcher were different, the influence of mischmetal addition on grain size of Mg-Al alloys should be the same. The main reason for the discrepancy ascribed to the difficultly etching technique for revealing the grain boundaries of casting magnesium alloys. Li et al. [38] reported that small amount addition of mischmetal ranging from 0.10 wt% to 1.20 wt% (mass fraction) causes considerable grain coarsening in Mg-Al alloys. After adding 1.20 wt% (mass fraction) mischmetal into AZ31, AM60 and AZ91 alloys respectively, the average grain size is approximately twice as larger as that of the original alloy. The change of microstructure must cause the change of mechanical properties of cast Mg-Al alloys.
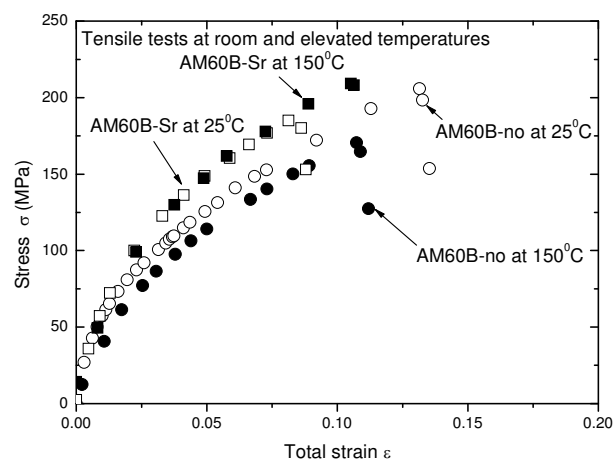
(A) Stress versus strain of AM60B
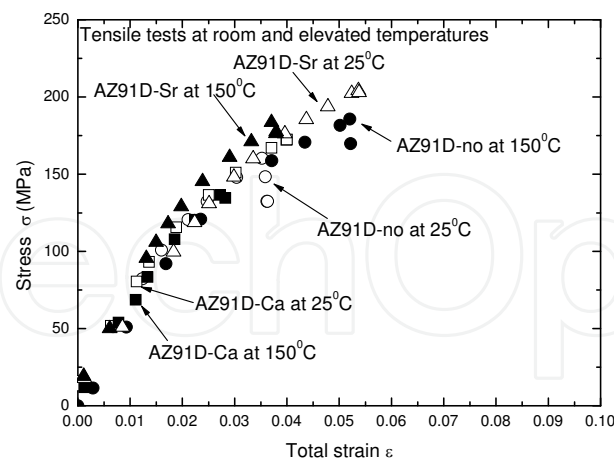
(B) Stress versus strain of AZ91D

Fig. 5. The tensile behavior of typical cast magnesium alloys

We previously reported that with increasing the amount of addition Ca into AZ91D, the hot-crack property decreases but the α-Mg grain-refinement of AZ91D alloy was improved [9-11]. The hot-cracking mechanism of Ca addition into AZ91D alloy was conjectured to be that Ca addition elevates the tendency of the divorce eutectic and formation temperature of the

Al$_2$Ca phase. The Ca-contained phase was distributed as a net-shape on the grain boundary and debases the boundary tension of liquid film, deteriorating the filling capacity and lowering the hot-crack property of cast magnesium alloys [9,11]. The influence of addition Sr on the microstructure of Ca-containing AZ91D alloy is shown in Figs. 3C. The Sr element aggregates also to the grain boundary just as Ca element does. Some of Ca element combined with Sr and formed a certain compound phase labeled MgAlCaSr phase. Sr addition to Ca-containing AZ91D alloy effectively suppresses the influence Ca addition on AZ91D alloy, which can assist in improving hot-crack resistance of Ca-containing AZ91D alloy. The effects of Ca/ Sr separate and composite additions into cast AZ91D magnesium alloy on the microstructure and tensile behavior indicated that Ca refines both grain and eutectic phase of AZ91D magnesium alloy. However, Sr can weaken the refinement effect of Ca when Ca/ Sr composite is added. Ca/ Sr addition evidently improves the microstructural stability of AZ91D magnesium alloy at elevated temperature. Addition of small Ca amount into AZ91D magnesium alloy improves yield strength but decreases the elongation of this alloy. Appropriate Ca/ Sr composite addition into AZ91D magnesium alloy can improve the elongation and maintain the excellent yield strength of AZ91D magnesium alloy containing Ca. It is deduced that separate Ca addition to AZ91D magnesium alloy is able to refine grain size and consequently improve the yield strength, based on the Hall-Petch relation, which is shown in Fig. 6. With decreasing the α-Mg grain diameter (d), the yield stress increased at the range from 170 μm ($\frac{1}{\sqrt{d}} = 0.077$) to 110 μm ($\frac{1}{\sqrt{d}} = 0.095$) in the different temperatures as shown in Fig. 6. The differences in segregation of Ca and Sr in a diffusion layer ahead of the advancing solid/ liquid interface during solidification affects the process of grain growth, which may result in grain size variation. Ca possesses strong segregation ability in the melt alloy and can promote an intensive constitutional under cooling during cooling in a diffusion layer ahead of the advancing solid/ liquid interface that restricts grain growth [10].
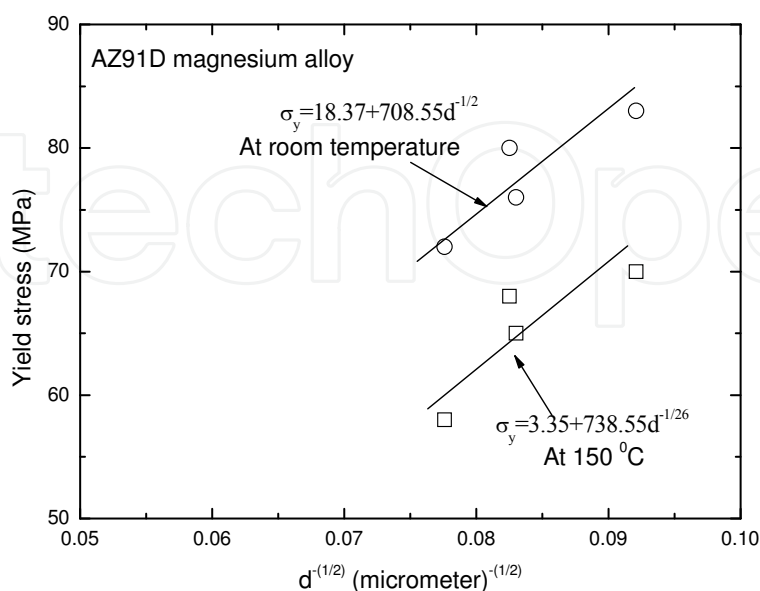

Fig. 6. Yield stress at different temperatures versus the diameter of d

2.3 Low-cycle fatigue cracking mechanism
2.3.1 Fatigue cracking mechanism at room temperature

Based on the above mentioned microstructural features of typical cast magnesium alloys, including addition Ca/ Sr or RE elements into these alloys, the low-cycle fatigue (LCF) crack initiation and propagation tests were carried out at RT by using scanning electron microscopy. Majority experiment results indicated that the fatigue crack initiation occurred preferentially at the pores, grain boundary because of the slip incompatibilities between adjacent dendrite cells as shown in Figs.7 [6,12,13-17]. In the Figs. 7A, the fatigue crack initiation occurred at the root of manual notch which its radius is about 50 μm and it is slightly larger than the average size of α-Mg grain of cast AM50 alloy. The micro crack propagated in interdendritic regions, along crystallographic planes. The propagation behavior of small fatigue crack depended strongly on the effect of both high temperature and microstructure. When there is a pore as shown in Figs. 7B, the crack occurred at the pore and accompanied by slight plastic deformations in the adjacent α-Mg grain surface. Another aspect of cracking shows in Figs. 7C, which shows that the crack initiation mechanism of general cast magnesium alloys is due to the plastic deformation incompatibilities to occur at the boundary or pores between the adjacent grains. Even if there are not the slip vestiges on the surface α-Mg grains under the applied stress, the crack occurred also at the boundary because the deformation mismatch between the α-Mg phase and β-$Mg_{17}Al_{12}$ phase as shown in Figs. 7D-7F. One of important reasons is caused by the difference of micro-hardness between both two phases [6,13-16]. As this reason, the fatigue crack propagated mainly along the boundary or β-$Mg_{17}Al_{12}$ phase of cast magnesium alloys at the RT as the typical cases shown in Figs. 8. The fatigue crack propagation process of cast typical AM50 alloy indicated that the crack propagated microscopically in the zigzag manner but macroscopically in a projection to the loading direction. With increasing of cyclic number under the maximum applied stress of 128 MPa ($\sigma_{max} / \sigma_{0.2} = 0.95$) at R=0.1, the fatigue

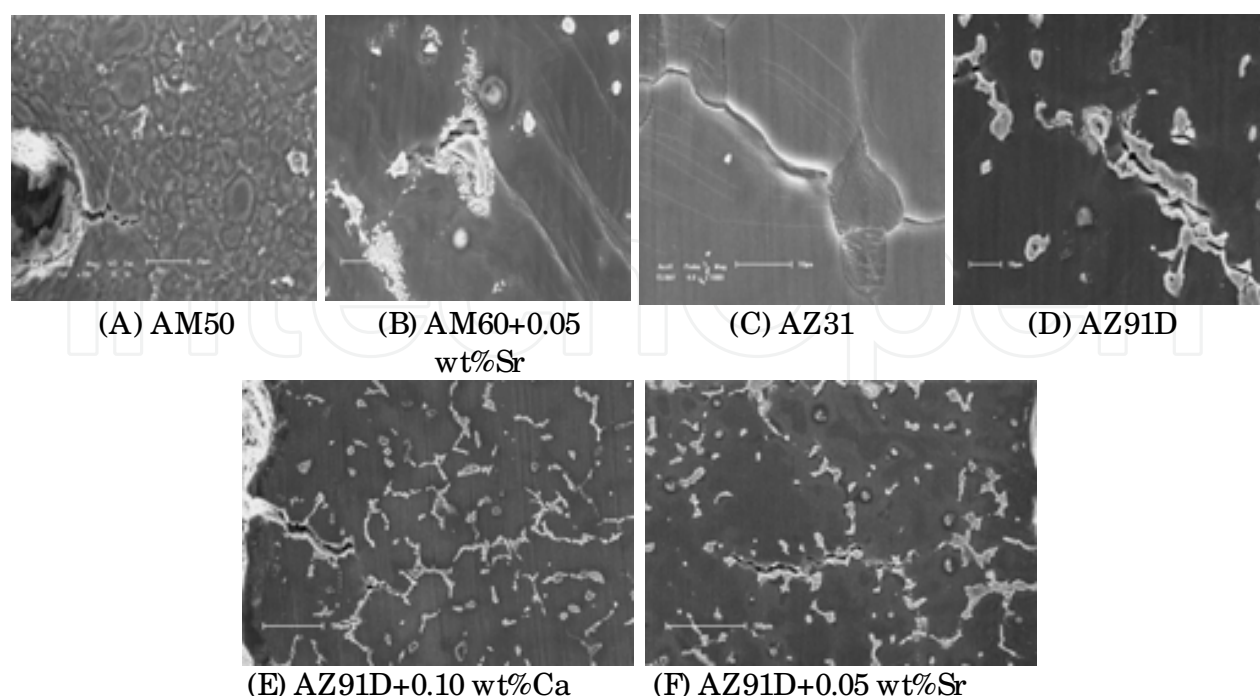|			
(A) AM50	(B) AM60+0.05 wt%Sr	(C) AZ31	(D) AZ91D

(E) AZ91D+0.10 wt%Ca	(F) AZ91D+0.05 wt%Sr

Fig. 7. Micro fatigue cracking images of different cast magnesium alloys at R=0.1

crack propagation path in front of a α-Mg grain resulted a deflective angle then around the boundary of this grain after N=5060 cycles as shown in Figs. 8C, this fatigue crack propagation direction evolved gradually a macroscopical crack after N=5222 cycles as shown in Figs. 8D. As the fatigue crack propagation test of cast AM50 alloy, the fatigue crack initiation occurred in the root of notch and propagation was along the boundary of α-Mg grain or interface between α phase and β phase as shown in Figs. 7C and 7D. In addition, the fatigue crack initiation and propagation accompanied always by the obvious plastic deformation vestiges, where occurred mainly on α-Mg phase surface as shown in Figs. 7B and 7C.

(A) N=4181, 33.9 μm   (B) N=4612, 44.9 μm   (C) N=5060, 70.5 μm   (D) N=5222, 95.5 μm
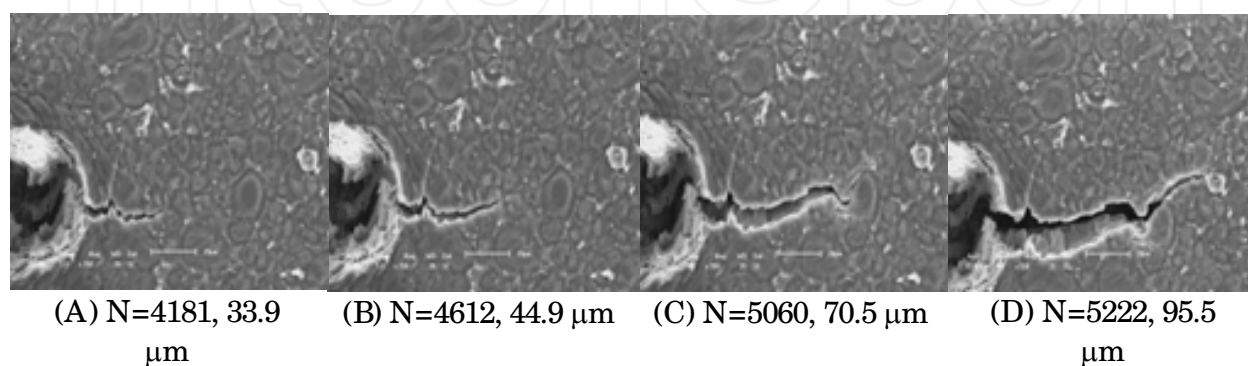
Fig. 8. Fatigue crack evolutive process of cast AM50 alloy at RT.

For majority investigations on the fatigue crack initiation and propagation of cast magnesium alloys, their fatigue cracking mechanism has the similar result at room temperature. For example, the fatigue crack initiation of cast AM60 alloy occurred also at the root of manual notch as shown in Figs. 9A, where accompanied by some plastic deformation vestiges around the fatigue crack. With increasing the cycles, the fatigue crack propagated along the boundary or β-$Mg_{17}Al_{12}$ phase compared with the results in Figs. 9A and 9B. In addition, the incontinuous crack initiated points were gradually linked as a main fatigue crack or to be defined as the Stage II of fatigue crack growth as shown in Figs. 9B with increasing of cyclic numbers. A larger number of studies devolving on microstructural observations have been conducted, however, and these allow us qualitatively to describe fatigue initiation as it is found to take place in the majority metallic materials. Fatigue fractures in these materials originate almost exclusively at internal or external surfaces, the latter being more common. In all materials there are regions of local inhomogeneity, that result in local "softening," or surface defect to cause local stress concentrations. Either or both of these factors can result in localized plastic flow, which, under the action of a cyclical stress (/ strain), can produce surface features that bear, in some senses, a resemblance to a crack or flaw. The plastic vestiges around the crack to be about 45° tilted to the applied loading as shown in Figs. 9A, in which indicated that the "extrusions" and "intrusions" occurred on the surfaces of α-Mg grains. We note that this nucleation stage, Stage I, of fatigue fracture is crystallographic in nature; that is, it is dictated by flow, rather than by tensile fracture, considerations. As a consequence, the initial fatigue crack plane normal is not parallel to the principal tensile axis, and the nucleated crack propagates initially at an angle other than 90° to this axis. Following these nucleation and initial crack-propagation events, slow crack growth (Stage II of fatigue) ensues after the Stage I crack has grown to

some critical size determined by material mechanical properties and the applied stress level and state as shown Figs. 9B.

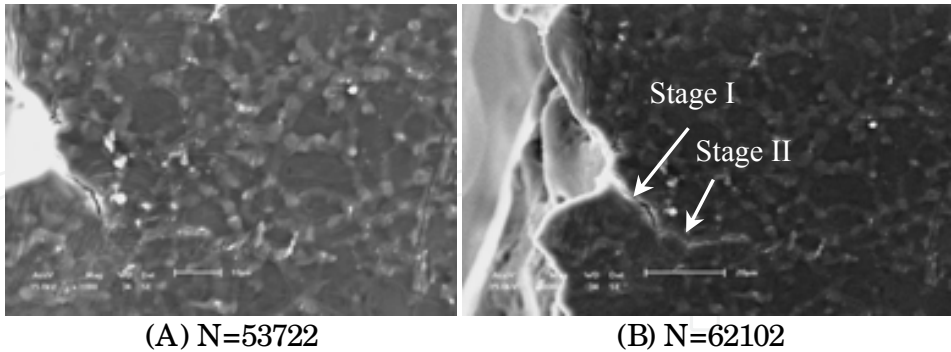(A) N=53722   (B) N=62102

Fig. 9. Fatigue cracking images of cast AM60 alloy under applied stress of 120 MPa at R=0.1.

The relations of all fatigue crack growth lengths versus the cyclic numbers can be expressed by $d\ell / dN \propto \ell$ when the applied stress is a constant. As the typical curves of cast AM50, AM60B and AZ91 alloys, the fatigue crack growth length shown in Figs. 10 at the different applied stress levels in a single log-coordinate system. For the cast AM50 alloy, the micro cracks growth lengths of $\log \ell$ are almost proportional relations to the cycles under the different applied stresses and the crack growth lengths can be effectively measured from 2 μm to 400 μm by using the SEM *in-situ* observation technology as shown in Figs. 8. With increasing of the maximum applied stress in these crack growth curves, the slope of fatigue crack growth curves is also to become larger and larger as shown in Figs. 10A. If we let to do the first derivative to the crack growth length in these curves, the relation of $d\ell / dN \propto \ell$ (the maximum applied stress is a constant) can be obtained. In addition, there is a slight difference in the slope of fatigue crack growth curves for both AM60B and AZ91 alloys under the same applied stress of 120 MPa, which indicated that the fatigue crack growth rate is not only dependence on the applied stress levels, but also dependence on the mechanical properties of cast magnesium alloys as shown in Figs. 10B.

(A) Crack length versus cycles of AM50 alloy   (B) Crack length versus cycles of AM60B and AZ91 alloys
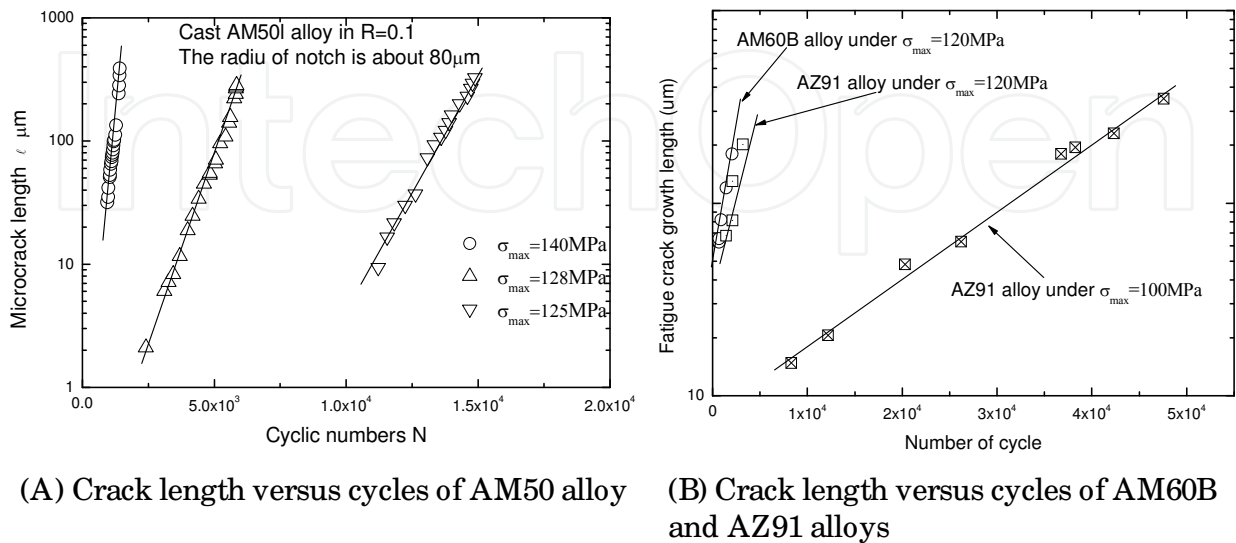
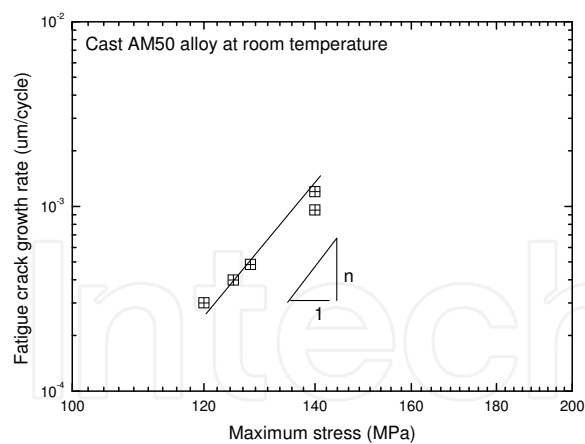Fig. 10. Crack growth length versus cyclic number of cast magnesium alloys.

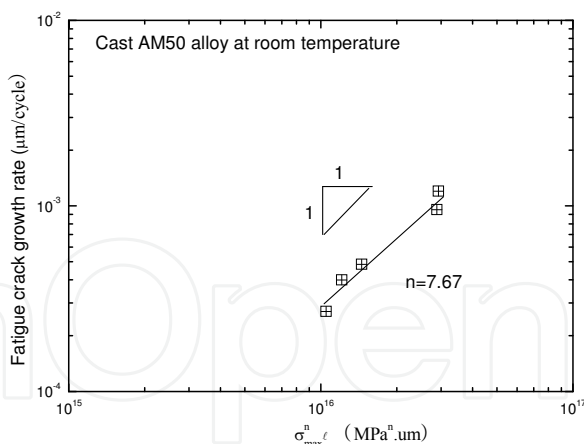Fig. 11. $d\ell / dN$ versus $\sigma_{\max}$ stress

Fig. 12. $d\ell / dN$ versus $\sigma_{\max}^n \ell$

As the curves of the fatigue crack growth at different conditions, if the crack growth length is as a constant, such as $\ell = 1$, we can obtain the linear relation of crack growth rate versus the maximum applied stress in the double logarithmic coordinates as shown in Fig. 11. The slope of linear curve is about 7.67 that it indicates that the fatigue crack growth rate can be quantitatively and effectively expressed by the term of $\sigma_{\max}^{7.67}$ when the fatigue crack growth length is one. Therefore, synthetically considered the effect of fatigue crack growth length and applied stress level on the fatigue crack growth rate, the curve about fatigue crack propagation tests of cast AM50 alloy at RT can be plotted as shown in Fig. 12. The slope of the curve is about 1.050, which means that the fatigue crack growth rate of cast AM50 alloy can be quantitatively and effectively characterized by the term of $\sigma_{\max}^n \ell$, where n=7.67. Therefore, the relationship between the fatigue crack growth rate and the term is written as following:

$$d\ell / dN = C\sigma_{\max}^n \ell \qquad (4\text{-}1)$$

where C is 3.16×10^{-20} (cycle/(MPa)^n) for cast AM50 alloy at room temperature. The constants (C, n) in Eq. (4-1) depend strongly on the experimental conditions and the mechanical properties of cast magnesium alloys, which are the cast magnesium alloys, temperatures, environments and applied loading types, such as push-pull, bending loading, and the stress ratio R etc., respectively. Especially the slight change of the index n will cause the larger change of the constant C. Therefore, the higher precision of experimental data is possible for SEM *in-situ* measurements of the fatigue crack growth tests of cast magnesium alloys.

Based on the both parameters of applied stress level and measurable crack growth length in this empiric equation, which involves to the ultimate capable measurement of fatigue crack length ℓ_0 to allowing the fatigue crack growth length ℓ_n of structural element, we can simply predicate the fatigue crack growth life of cast magnesium alloys as following:

$$N_c = \int_{\ell_0}^{\ell_n} \frac{d\ell}{C\sigma_{\max}^n \ell} = \left(\frac{\log \ell}{C\sigma_{\max}^n} \right) \Bigg|_{\ell_0}^{\ell_n} = \frac{\log \ell_n - \log \ell_0}{C\sigma_{\max}^n} \qquad (4\text{-}2)$$

Above mentioned the estimation of fatigue crack growth life, there is an obvious benefit that the fatigue crack growth law is rather simple because it is based on the engineering stress amplitude or maximum stress at the certain stress ratio and the measurable crack growth length. In addition, as a general engineering fatigue life of materials, it is able to include to two parts of fatigue life, one is the fatigue crack initiated life and another is the fatigue crack propagation life. The farmer is mainly to be decided by the fatigue experiments of smooth specimens or to be deduced by *S-N* curves of smooth specimens. The latter is mainly to be estimated by the fatigue crack propagation experiments with the notch specimens. And it is necessary that considering the effects of experimental and environmental conditions including to the effect of modeling method on the fatigue life of cast magnesium alloys.

2.3.2 Fatigue cracking mechanism at elevated temperature

As above mentioned results that the fatigue crack initiation and propagation behavior of cast AM50, AM60, AZ91 alloys are at room temperature. In this section, we introduce simply the effect of the elevated temperature on the fatigue crack initial and propagated mechanism of typical cast magnesium alloys. For example, Figs. 13 shown that the typical fatigue cracking features of cast AM50 alloy at the different elevated temperatures but under the same applied stress of 125 MPa. In the Figs. 13A, the fatigue crack initiation occurred still at the root of notch but the early stage of crack propagation is along either the boundary of α-Mg grain or to cleave the α-Mg grain in front to the crack tip. The fatigue cracking mechanism in the microscopically zone is analogous to the quasi-brittle or quasi-ductile (intervenient brittle and ductile) fracture mechanism of engineering materials. At room temperature, we did not find that the α-Mg grain of cast AM50 alloy was cleaved. However, the fatigue crack propagation is either along the boundary of α-Mg grain or to cleave the α-Mg grain as shown in Figs. 13C. In addition, the fatigue crack propagation mechanism of cast AM50 alloy at the elevated temperature indicated that the fatigue branch crack was found as shown in Figs. 13B. This means that the fracture mechanism of cast magnesium alloy at the elevated temperature which is dominated by the couple of Mode I and Mode II, which differs obviously from that which is main fracture Mode I at room temperature in microscopically zone. Although the cyclic force acting normal to the crack surface serves to open up the crack and to propagate it in a direction normal to the tensile stress, a shear component of stress is applied normally to the leading edge of the crack, which propagates in a direction parallel to the sense of the applied stress to be caused by the plastic deformation in local region at the elevated temperature state. Therefore, the branched probability of fatigue crack is along about 45° tilted to the crack propagation direction as shown in Figs. 13B. This is because there is the maximum shear component of applied normal stress in this direction. Corresponding effect of the elevated temperatures on the fatigue cracking mechanism of cast magnesium alloys has analogous to composite fractures Mode I/ II. Therefore, the effect of the elevated temperature on the fatigue cracking mechanism of cast magnesium alloys can be not ignored. This effect of the elevated temperature on the fatigue branched cracking can be contributed by the hardness of β-$Mg_{17}Al_{12}$ to have a softness trend so that the plastic deformation mismatch in the boundary or interface becomes decreasing or weak. This is a competitive result of the interface strength and the fracture strength of α-Mg grain.

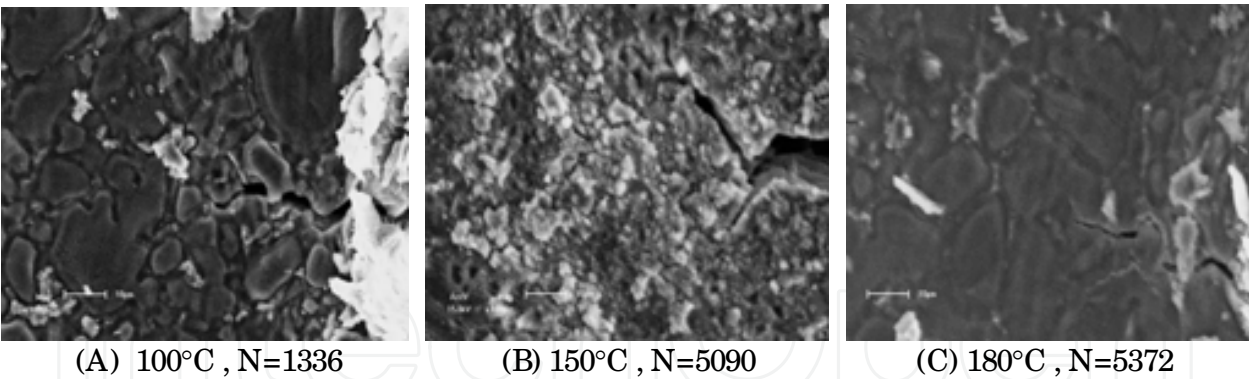| (A) 100°C , N=1336 | (B) 150°C , N=5090 | (C) 180°C , N=5372 |

Fig. 13. Fatigue cracking characterizations of cast AM50 alloy at the elevated temperatures under the maximum applied stress of 125MPa at R=0.1.

All typically measured results of fatigue crack propagation length of cast AM50 alloy at the different elevated temperatures according to the projection to the loading direction can be plotted in Figs. 14. These curves of fatigue crack growth length at the different elevated temperatures are still similar to the linear trends under the different applied stress levels. It means that the fatigue crack growth rate ($d\ell / dN$) is also the direct proportion the fatigue crack growth length (ℓ) when the applied stress is a constant. Therefore, if the fatigue crack growth length is a constant, the relationship between the fatigue crack growth rate and the applied stress amplitude at the different elevated temperatures can be plotted as shown in Fig. 15. These slopes of curves of cast AM50 alloy at the different elevated temperatures slightly decreased with the increasing the elevated temperatures, which are 7.67 at room temperature, 6.63 at 100 °C, 6.55 at 150 °C and 6.20 at 180 °C. It means that cast magnesium alloy was intenerated with increasing the temperatures. Synthetically considering the interactional effect of the fatigue crack growth length and the applied stress levels at the different temperatures, the fatigue crack growth rate can be also characterized by the term of $\sigma_{max}^{n}\ell$, which is similar to that at the room temperature, as shown in Fig. 16. It is clearly seen that the elevated temperatures caused not only the slight change of index of fatigue crack growth rate but also main influence the constant of C in Eq. (4-1). The higher of the elevated temperature is, the larger of C is as shown in Fig.18. That is, the fatigue crack growth rate at the higher elevated temperature is faster than that at the lower elevated temperature because of the slight difference in the fatigue cracking mechanisms.

| (A) Crack length versus cycle at 100°C | (B) Crack length versus cycle at 180°C |
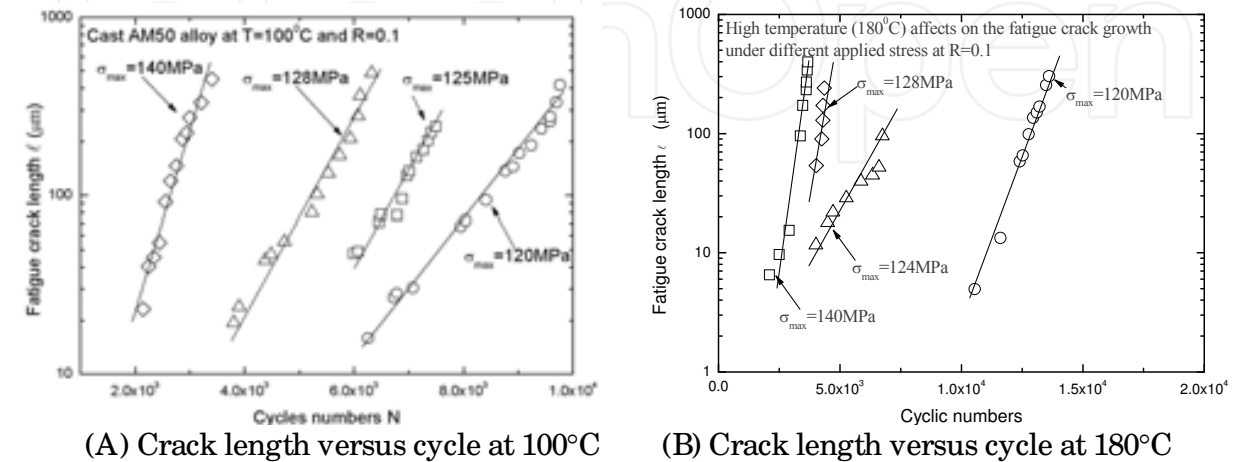
Figs. 14. Crack growth length versus cyclic number at the elevated temperatures
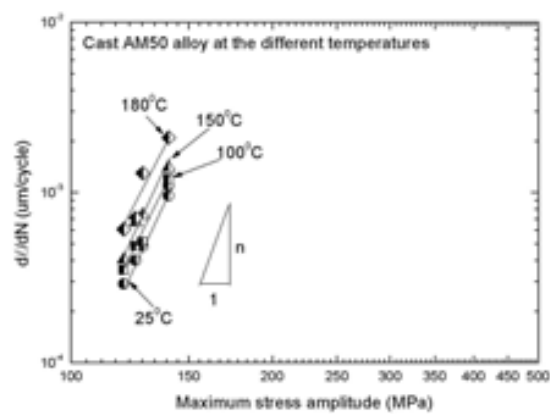
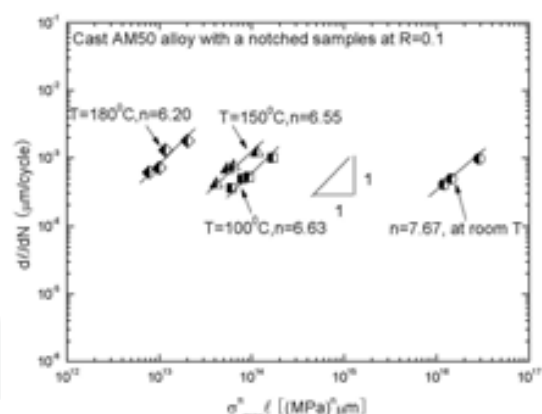Fig. 15. $d\ell / dN$ versus $\sigma_{\max}$

Fig. 16. $d\ell / dN$ versus $\sigma_{\max}^{n}\ell$

At the different elevated temperatures, the dominated index n in fatigue crack growth rate can be estimated by the linear function of $n = 7.78 - 9 \times 10^{-3}T$ as shown in Fig. 17. The variations of power index n versus different elevated temperatures can be explained by the difference of yielding stress and mechanism of small fatigue crack growth at different temperatures. And the constant in Eq.(4-1) versus the elevated temperatures can be estimated by the $\log C = -24.56 + 3.62 \log T$ as shown in Fig. 18. Therefore, the fatigue crack growth rate of cast AM50 alloy at the different temperatures can be also predicated by Eq.(4-1).

Measurements or estimation of the crack growth rates are useful for an engineering design, and they also add to our understanding of the fatigue process. For example, knowledge of the Stage II as shown in Figs. 9B crack-growth arte and the cast magnesium alloys' fracture toughness permits an estimation of the number of Stage II cycles prior to catastrophic final fracture. Thus, for a cast magnesium alloy subject to LCF ($N \leq 10^3 \sim 10^4$ cycles), for which Stage II occupies a majority portion of the cast magnesium alloy's life, the number of fatigue cycles it can withstand prior to failure can be approximated. Moreover, as discussed in the above section of microstructural features of cast magnesium alloys, many structural members contain preexisting surface flaws or cracks that can be precursors to fatigue (tensile) failure, and which eliminate the necessity of nucleating a fatigue crack. For these, knowledge of the critical flaw size and its geometry also allows estimation of fatigue lifetime.
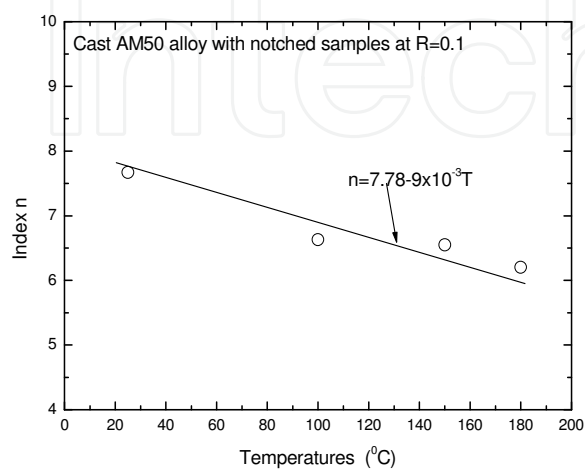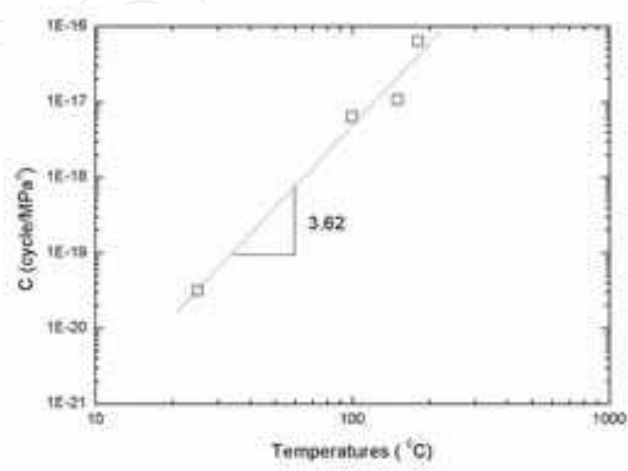

Fig. 17. Index n in Eq. (1) versus Ts

Fig. 18. Constant C versus Ts

Measurement of Stage II crack growth rates are commonly performed in many laboratories. A pre-notch sample of the kind used for fracture-mechanics tests (cf. in next section of 2.4) suffices also for the measurements of fatigue-crack growth rate. The sample is typically subjected to a fixed stress (or in some cases, strain) amplitude at a specified mean stress or stress ratio (R), and the crack growth length is monitored as a function of the number of cycles. Crack growth length can be measured in a variety of ways, including direct measurement with an optical microscope or by measuring the electrical resistance across the fractured portion of the sample or indirect measurement with the plastic replication method, accompanied by a suitable calibration procedure. These results obtained from such testing are illustrated in Figs. 8, Figs. 10 and Figs. 14. Except to recognize the fatigue crack growth rates of materials can be expressed by the above term ($\sigma_{max}^n \ell, \Delta\sigma^n \ell, \sigma_m^n \ell$, $\Delta\sigma$ is a stress range and σ_m is a mean stress etc.), the fatigue crack (Stage II) growth is driven principally by the same kinds of forces that are responsible for tensile fracture. The driving force of crack growth is dependence on the particular cyclical stress history and stress intensity, which scales with the product of stress and the square-root of crack length. When extended to fatigue fracture, the same approach is taken, with the exception that, in recognition of the necessity of a cyclical stress for fatigue, the stress range $\Delta\sigma$ substitutes for σ in the stress-intensity factor (SIF). In fact, a larger number of studies have shown that, for a given material and stress ratio, Stage II crack growth rates are a unique function of $\Delta K (\sim \Delta\sigma(\ell)^{1/2})$, and that over an appreciable range of this variable, $d\ell / dN$ is related to it by Paris [40]

$$d\ell / dN = A\Delta K^m \tag{4-3}$$

Where A is a constant that depends on the material and the stress ratio, and m is an empirical constant ($2 \leq m \leq 4$, usually) deduced from crack-growth rate measurements.
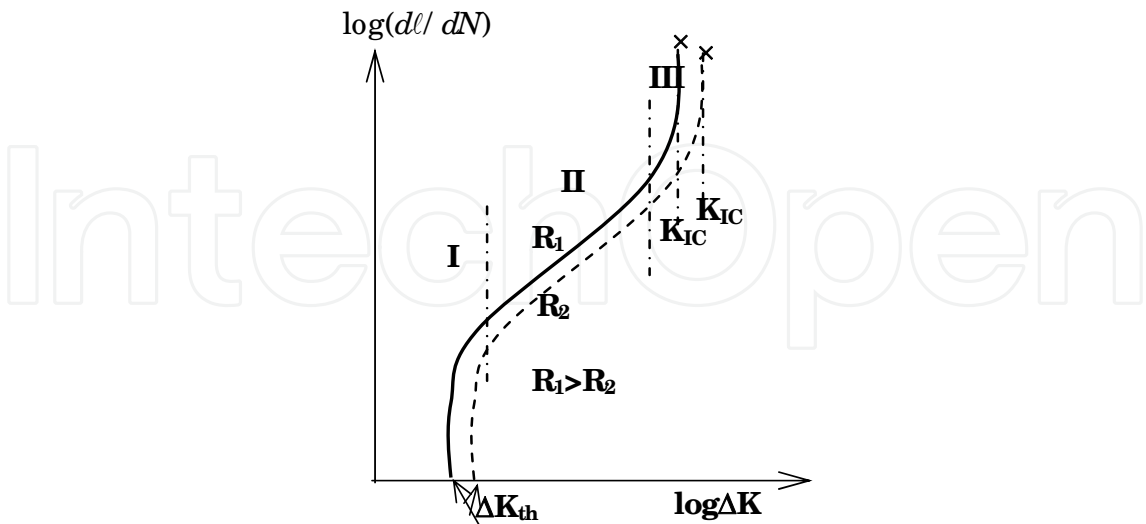

Fig. 19. Schematic of crack-growth rate as a function of the cyclical stress intensity factor for different R values ($R = \sigma_{min} / \sigma_{max}$)

Although $d\ell / dN$ of materials may be uniquely as a function of ΔK, it must be emphasized that Eq. (4-3) applies only over a portion of the $d\ell / dN - \Delta K$ curves as similar to above

mentioned method which used by the term of $\sigma_{max}^{n}\ell$. This is made clearer by consideration of Fig. 19, which shows both schematic plots of $d\ell/dN - \Delta K$. From these figures we see that at low ΔK values, crack growth rates are very low (Stage I, as shown in Figs. 9). Indeed, it appears there is a threshold value of ΔK ($=\Delta K_{th}$) below which Stage II fatigue cracks cannot realistically propagate. This value, ΔK_{th}, represents inherently safe design against fatigue fracture. Unfortunately, ΔK_{th} is so low in comparison to critical stress intensities (typically 5~10 per cent of them) that use of engineering materials at such low ΔK values represents a great restriction on their effective utilization. Current engineering design, therefore, is to accept the presence of fatigue cracks in most structures, to assume that some of them will propagate, but to insure, also, that they will not grow to catastrophic length during the intended lifetime of the part. In contrast, if the critical crack growth rate is defined as 10^{-10} m/ cycle (ASTM: E647, 1998) [41], we can decide the value of ΔK_{th} or the term of $\sigma_{max}^{n}\ell$.

(A) $d\ell/dN - \Delta K$ at 25°C and 100°C   (B) $d\ell/dN - \Delta K$ at 150°C and 180°C
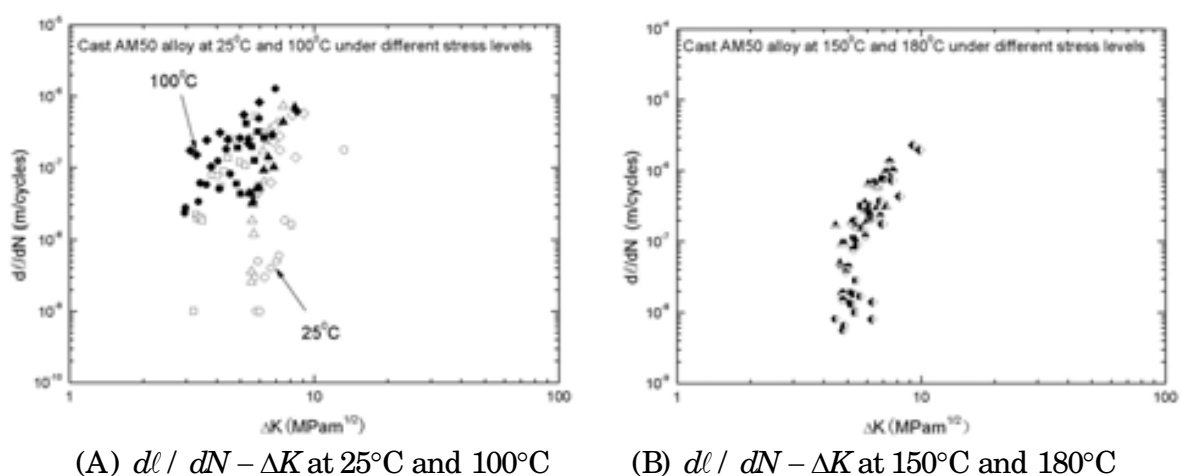
Fig. 20. Crack growth rate as a function of SIF at the different temperatures.

Therefore, based on the results of fatigue crack propagation tests at the different elevated temperatures and SIF, the experimental results were plotted as shown in Figs. 20. These results have a larger scatter at RT and 100 °C than that at over than at 150 °C when the maximum applied stress amplitudes are 120 MPa, 125 MPa, 128 MPa and 140 MPa, respectively. It means that the fatigue crack growth rate at both RT and 100 °C can not be characterized uniquely by SIF as shown in Figs. 20A although the fatigue crack growth rate can be uniquely characterized by the term of $\sigma_{max}^{n}\ell$ at the different temperatures as shown in Fig. 16, respectively. However, these results indicated that the fatigue crack growth rate can be simply estimated by SIF at the elevated temperatures from 150° to 180°C as shown in Figs. 20B, which is because the fatigue crack growth mechanism is similar at the higher temperatures. In addition, it is still difficult to evaluate the fatigue crack growth rates of cast AM50 alloy uniquely and reliably based on the SIF at different elevated temperatures. With increasing of the maximum applied stress amplitude at the same temperature or with increasing of the temperature at the same applied stress, the fatigue crack growth rates are varied but they do not uniquely depend the ΔK as shown in Figs. 20A. When the temperature is over than 150 °C, the fatigue crack growth rate at the closer threshold ΔK_{th}, which is defined as 10^{-10} m/ cycle, can be uniquely decided by SIF with some scatters about it as shown in Figs. 20B.

Stress parameters needed to characterize the push-pull fatigue test (and other types of, such as rotating-beam fatigue test) are related to the maximum ($\sigma_{\max}$) and minimum ($\sigma_{\min}$) stresses the part is subjected to each cycle. These include the mean stress $\sigma_{mean} = (\sigma_{\max} + \sigma_{\min})/2$, the stress range $\Delta\sigma = \sigma_{\max} - \sigma_{\min}$, and the stress amplitude $\sigma_a = (\sigma_{\max} - \sigma_{\min})/2$. Frequently, the stress ratio $R = \sigma_{\min}/\sigma_{\max}$ is also used parametrically; clearly, R is redundant provided σ_{mean} and σ_a are known. For the rotating-beam fatigue test, we see that $\sigma_{mean} = 0, \Delta\sigma = 2\sigma_{\max}, \sigma_a = \sigma_{\max}$ and R=-1.

Only a few of structural parts prone to fatigue failure experience cycles that are simulated by alternating compression and tension stresses of equal magnitude. Thus, the tests other than the rotating-beam test are better suited for assessing the fatigue resistance of other parts. A cyclical tensile test is often suitable for this purpose. In it, a specified stress amplitude is cyclically imposed on a finite mean stress; a typical stress-time history for such a procedure is shown in Figs. 21.
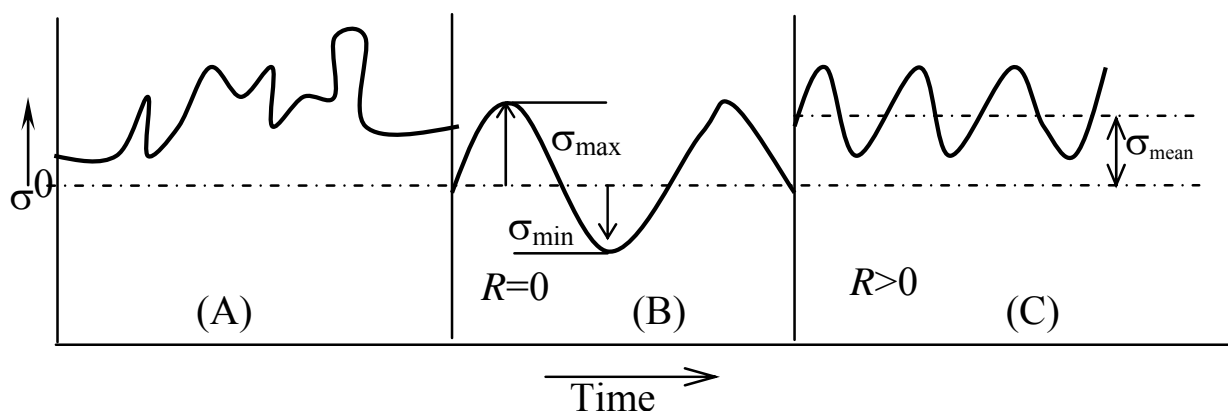

Fig. 21. Characteristic stress-time variations in (A) an engineered structure subject to a positive mean stress on which is superimposed random loading, (B) a rotation beam fatigue test in which the material experiences alternating compressive and tensile stresses of equal magnitude, and (C) a cyclical tensile test in which a time-varying sinusoidal stress is imposed on a constant mean stress.

Because of the important role of plasticity in fatigue damage, it is fundamentally more sounds to assess a cast magnesium alloy's fatigue response under different conditions of a specified cyclically applied strain, rather than stress. Nonetheless, stress-controlled tests are still traditional and are also conveniently performed; the results from them are widely used in engineering design against fatigue damage. Based on the results of stress-controlled tests, it is possible to estimate the relation of the cyclical stress-strain of cast magnesium alloys. For example, during high-cycle fatigue (HCF) (when the number of cycles to failure is very larger ($>10^3 \sim 10^4$)) the macroscopic stress level is such that the structure as a whole undergoes only elastic deformation, and, in this case, the elastic strain range ($\Delta\varepsilon_e$) is coupled to the stress range by:

$$\Delta\varepsilon_e = \Delta\sigma/E \qquad (4\text{-}4)$$

where E is the elastic modulus of a cast magnesium alloy. Conversely, in the low-cycle fatigue range, the cast magnesium alloy is typically subject to the plastic strain in

macroscopic and microscopic scales. For relatively low values of N_f, the plastic strain range is as following:

$$\Delta \varepsilon_p = \Delta \varepsilon_t - \Delta \varepsilon_e \qquad (4\text{-}5)$$

where $\Delta \varepsilon_t$ is a measurable total strain value by a strain sensor. $\Delta \varepsilon_e$ is calculated by and applied stress range according to the Eq. (4-4). Sometimes, the plastic strain range of some cast magnesium alloys (if the ratio of $\sigma_{\max} / \sigma_{0.2} > 0.75$) is much greater than the elastic one, so that

$$\Delta \varepsilon_t \approx \Delta \varepsilon_p \qquad (4\text{-}6)$$

Therefore, the plastic strain range is related to applied stress range by knowing the cast magnesium alloys' cyclical hardening response. In the general case, the plastic strain range is still decided by Eqs. (4-4) and (4-5). Thus, the strain is also as a simple function of the term of $\sigma_{\max}^n \ell$, such as $\Delta \varepsilon_p^{n'} \ell$. Although elongation of majority of cast magnesium alloys is less than 15%, the accumulated plastic deformation is very important for evaluating the fatigue damage especially in elastic-plastic deformation region. The relationship between the applied stress and response strain of cast magnesium alloy in LCF damage process can be expressed by the Ramberg-Osgood model [42] as

$$\Delta \varepsilon = \frac{\Delta \sigma}{E} + (\frac{\Delta \sigma}{k})^{1/m} \qquad (4\text{-}7)$$

where k is a constant of the cast magnesium alloy. And m is hardening coefficient of a cast magnesium alloy, in general, $0 < m < 1$ [43].

Cast magnesium alloys behave "differently" when subjected to a cyclical stress-strain environment from the way they do when subjected to a monotonously increasing stress or strain as in a tension test. Knowledge of this cyclic behavior enhances our understanding of the fatigue process. Moreover, data obtained from such studies are useful for engineering design against fatigue fracture. The fatigue behavior of cast magnesium alloys under a cyclical mechanical environment can be investigated by subjecting them to either specified cyclical stress or strain amplitude. The latter is more commonly done and the results from this kind of test constitute the focus of our discussions. If fixed strain amplitude (consisting of some plastic strain component) is imposed on a cast magnesium alloy, the stress range is not fixed but varies with the number of cycles or strain reversals. The cast magnesium alloy may either soften (the stress amplitude decreases with increasing of time/ cycles) or harden (when it increases with number of cycles). Moreover, the extent of softening or hardening is a function of the plastic strain range. The behavior of a cyclically hardening material is illustrated in Figs. 22A. Hear we see that the stress amplitude required maintaining the specified strain range increases with the number of cycles, and this is also manifested by an increase in the area of the hysteresis loop (the trace of stress and strain over the course of one cycle). When the magnesium alloy cyclically softens as shown in Figs. 22B, the hysteresis loop becomes smaller concomitantly with the decrease in the stress amplitude necessary to maintain the fixed strain range.
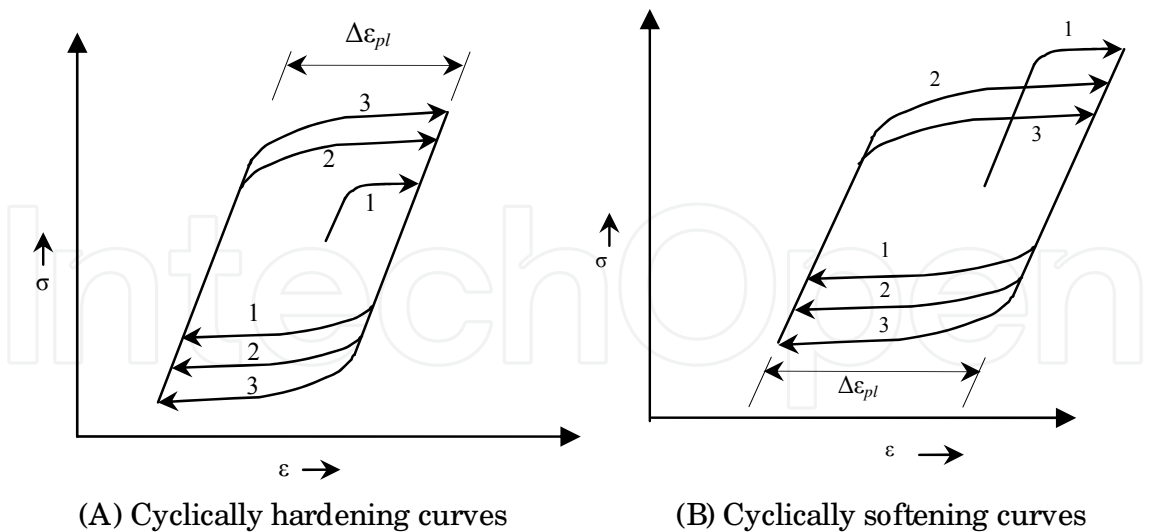
(A) Cyclically hardening curves   (B) Cyclically softening curves

Fig. 22. The hysteresis loop of materials

2.4 Experimental approach-based on SEM in-situ observation

As an investigation on the fatigue cracking mechanism of cast magnesium alloys relates to the microstructural features, the SEM *in-situ* observation is an impactful approach in the experimental studies. This real detects of fatigue small crack initiation and propagation of cast magnesium alloys were carried out using a specially designed the servo-hydraulic loading testing system in the vacuum chamber of SEM as shown in Figs. 23A. The specimen as similar to the dog-bone shape is put into the jig as shown in Figs. 23B and 23C. Then they are put into the chamber of SEM. To investigate the effect of elevated temperature on the fatigue cracking behavior of cast magnesium alloy, we can use the approach as shown in Figs. 23C and 23D. In this system, the controlled accuracy of temperature is less than ±3°C when the maximum temperature is 800 °C.

(A) System   (B) Jig at room   (C-D) Jig at high temperature
                  temperature

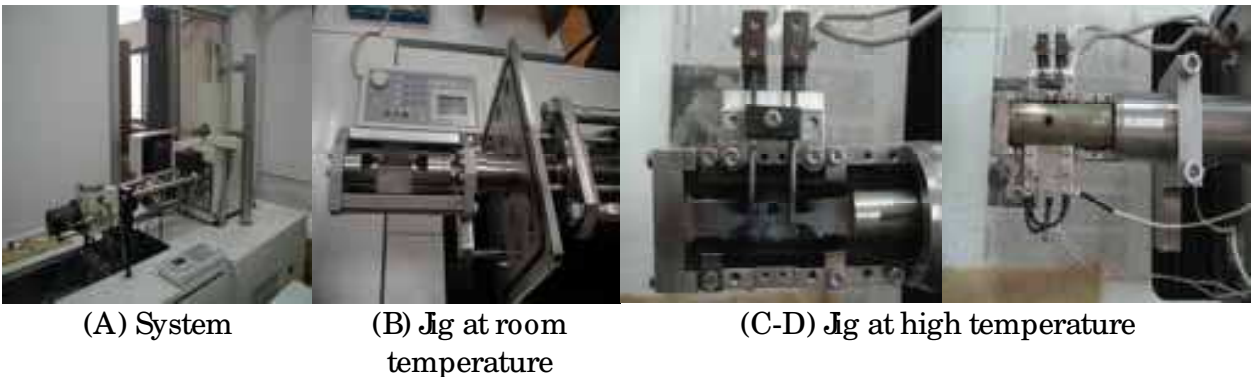Fig. 23. SEM *in-situ* observation and loading with the different jigs systems

All fatigue crack propagation tests are by the loading control at R=0.1 in this chapter. Therefore, the displacements and temperatures have to be performed by two computers. And the experimental data are also recorded in a random time during the fatigue test.

In addition, the system can provide pulsating, such as sine wave etc., loads at different frequencies about general not over than 10 Hz of a certain load capacity. Due there is a

deformation on the surface of sample under the applied loadings, it is difficult to observe the clear damaged characteristics in the microscope. Therefore, the special technique was used by Shimadzu Inc. Japan as shown in Figs. 24. Based on the principle of SEM *in-situ* observation, the fatigue micro crack initiation and propagation behaviors of materials become possible in the random cycles. That is, the signal of SEM was directly transferred to a computer via a direct memory access type A/ D converter, marking it possible to sample 960×1280×8 bit (or 1920×2560×8 bit) in one frame or over than frames of SEM images successively [13-18,44-48]. You can see why we can obtain the clear images from the presence of deformation specimen surface at less than 0.1 Hz based on the principle and skilled control technology.
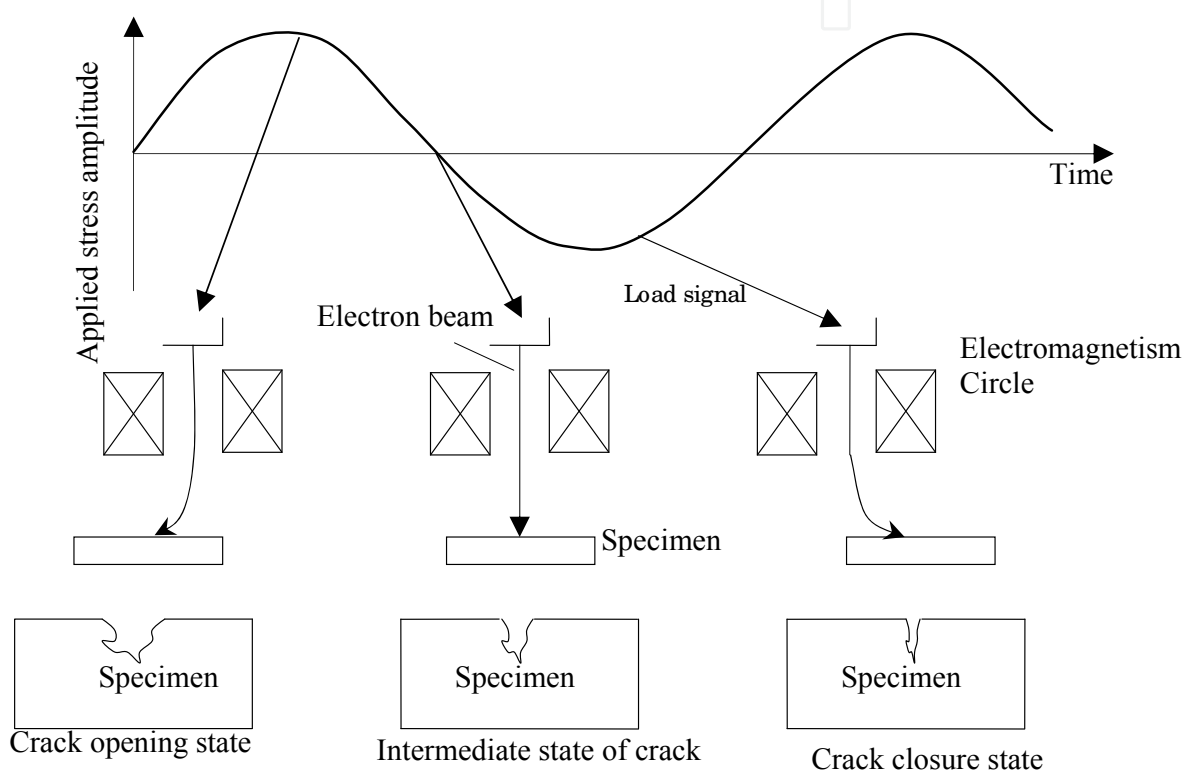
Fig. 24. The principle of SEM *in-situ* observation.

3. Effects of spacing and alignment pores on the fatigue cracking behavior of cast magnesium alloys

3.1 Fatigue cracking behaviors of cast magnesium alloys with the different spacings and orientations of two pores

As the typical plate with some pores in engineering applications and their especial mechanical properties of cast magnesium alloys, the effects of spacing and alignment pores on the fatigue cracking behaviors have to be considered as an issue in majority studies. Above mentioned the fatigue crack initiation behavior indicated that the effect of stress concentrate at a notch on the fatigue crack initiation can be not ignored. Therefore, the interaction of multi-cracks to occur at the multi-pores on the plate of cast magnesium alloys and the influence of intersectional stress concentrate regions between the multi-pores on the fatigue crack initiation and propagation are also not to avoid. These issues refer the

experimental and simulated methods, which can investigate the existent pores whether to contribute faster growth from the origins of crack. In this section, we investigated the effects of different spacing and alignments of manually small pores (as shown in Table 3) on the fatigue crack propagation and fracture behaviors of cast magnesium alloys based on SEM *in-situ* technology and simulation results.

Materials	Diameters of two pores (mm)	Spacing between two pores (mm)	Alignments of two pores	
			90° inclined pores	45° inclined pores
	0.50	1.00	√	√
AM60B	0.50	2.00	√	√
	0.50	3.00	√	√
	0.50	1.00	√	√
AZ91	0.50	1.50	×	√
	0.50	2.00	√	√
	0.50	3.00	√	√

Table 3. Spacing and alignments of small pores for cast magnesium alloys
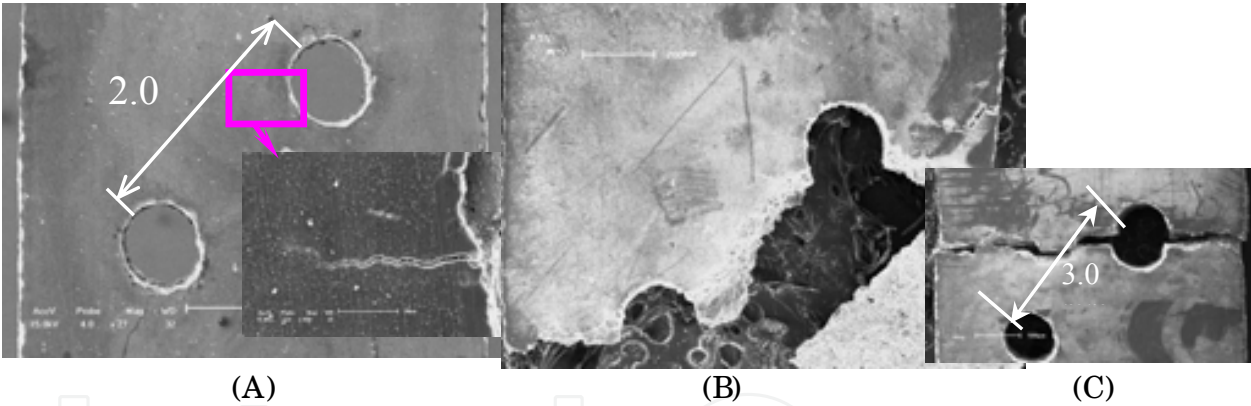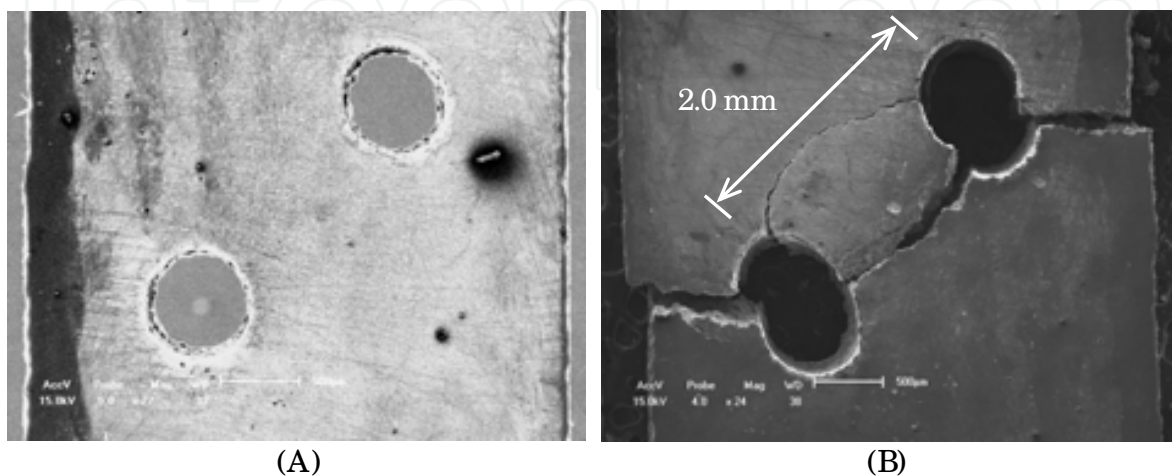

Fig. 25. Effect of 45° orientations at the two small pores on the fatigue crack growth behavior of cast AM60B alloy. (A) σ_{max}=100MPa, D=2.0mm, N=5000; (B) σ_{max}=100MPa, D=2.0mm, N_f=9744; (C) σ_{max}=100MPa, N_f=9075, D=3.0mm.

Figs. 25 given the typical fracture cases with two 45° orientations and different spaces under the same stress amplitude and *R*=0.1. The fatigue crack growth path of cast AM60B alloy is obviously different compared with the results both Figs. 25B and Figs. 25C. Before the cycles of about 5000, the early stage of one fatigue crack has occurred at the root of upside pore and the crack growth length is about 150 μm and its propagation direction is about 90° tilted to the applied loading direction. However, the crack propagation direction takes place the deflexion after 5100 cycles subsequently its fracture manner is as shown in Figs. 25B. With increasing the spacing between inclined two pores from 2.0 mm to 3.0 mm as shown in Figs. 25C, the fatigue crack propagation at one pore is different from the result as shown in Figs. 25B. These results indicate that the fatigue crack initiations are still to occur at the stress

concentrate regions in closed to the pores and the early stage of fatigue crack propagation is mainly dominated by fracture mode I. These fatigue crack propagation accompanied by the interaction between two inclined-pores. Therefore, the effect of the spacing of two pores on the fatigue fracture is not ignored although the experimental conditions are the approximately same such as the stress amplitude and with the 45° orientations of two pores. For this case, there is a critical spacing to cause the deflexion of fatigue crack propagation direction in the range from 2.0 mm to 3.0 mm, but which is not less than 2.0 mm.

(A)   (B)

Fig. 26. Effect of 45° orientations at the two small pores on the fatigue crack growth behavior of cast AZ91 alloy. (A) σ_{max}=145MPa, D=2.0mm, N=0; (B) σ_{max}=145MPa, D=2.0 mm, N_f=952.

As another typical case with the 45° orientations at the two pores specimen of cast AZ91 alloy, the fatigue crack propagation behavior is shown in Figs. 26A-26B when the applied stress level was changed at R=0.1. The spacing between the 45° orientations at the two small pores is still about 2.0 mm. The result indicates that fatigue crack initiation stochastically occurred at the root of one pore and the fatigue multi-cracks initiation to occur at the roots of two small pores. Thereinto, the fatigue crack in closed edge of specimen propagated along the 90° tilted the applied loading direction and the fatigue cracks between two pores easily produce a coalescence of crack with another one so that the fatigue cracks propagation directions have to deflect an angle in the stress concentration overlapped regions as shown in Figs. 26B. Compared with the results above mentioned cast AM60B, the different mechanical properties of materials (especially the fracture toughness) affect on the difference of fatigue crack propagation path at the approximately experimental conditions as shown in Figs. 25 and Figs. 26. For the specimens with two small pores tilted about 45° orientations to the applied loading axis, the fatigue crack propagation path depends not only on the spacing of two small pores, but also on the fracture toughness of cast magnesium. In contrast, the fatigue crack initiation and propagation behaviors follow as the principle of the maximum strength of material. That is, the fatigue crack initiation occurs at the region of stress concentration and the fatigue crack preferentially propagated along the overlapped region of stress concentration. In addition, the influencing range of two pores with 45° orientations on the fatigue crack growth path is the critical spacing value, which is not over than 2.0 mm when the diameter of pore is about 0.5 mm. If the smaller spacing of two pores is, the greater in the probability of the fatigue crack propagated interaction between two small pores. As the elongation of AZ91 is about 3%, which is less than that of

AM60B, the fatigue crack initiation easily occurs at the many sites around each pore even if there is a strong influence of stress concentrate region. Therefore, these multi-cracks propagated as the manner as shown in Figs. 26B. This reflects the fact that the fatigue crack initiation behavior is a competitive result of the interactions both fracture toughness properties and notch effect of cast magnesium alloys.
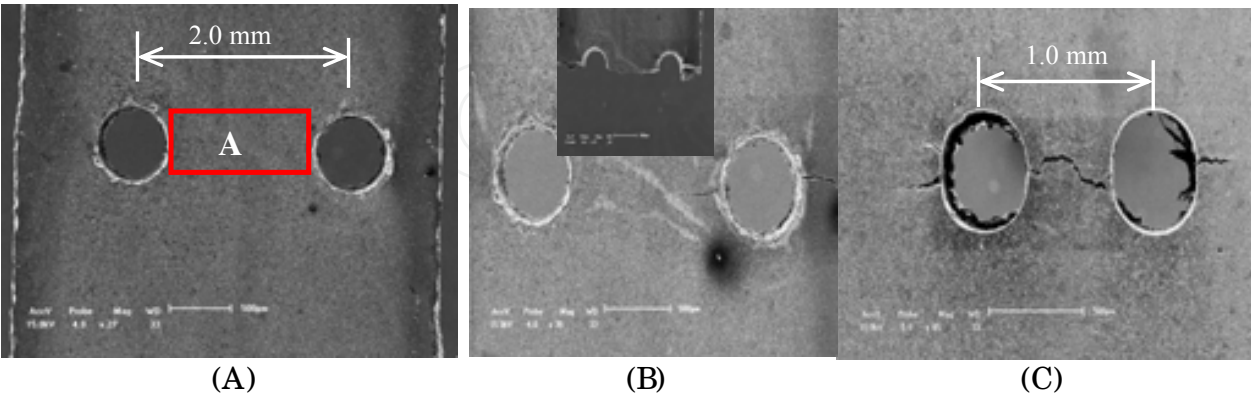

(A)　　　　　　　　　　(B)　　　　　　　　　　(C)

Fig. 27. Effect of 90° orientations at the two pores on the fatigue crack growth behavior of cast AZ91 alloy at R=0.1. (A) σ_{max}=100MPa, N=0; (B) σ_{max}=100MPa, N=52464; (C) σ_{max}=100MPa, N=38543.

Figs. 27A to Figs. 27C show the fatigue crack initiation and propagation behaviors of cast AZ91 alloy for the 90° tilted to the two small pores and the spacing of about 2.0 mm, 1.0 mm, respectively. These results indicated that the fatigue crack initiation occurred still at the root of notch in each pore. Due the spacing between two pores is greater than the distance to edge of sample, the fatigue crack propagated preferentially to the edge of sample as shown in Figs. 27B. However, if the spacing between two pores is less than 2.0 mm as shown in Figs. 27C, the fatigue crack propagation direction is preferentially to the insider between the two small pores (to refer the mark A zone in Figs. 27A). And the fatigue cracks to occur at the sides between the two pores were easily linked a main fatigue crack so that it cause rapidly the fatigue fracture of specimen as shown in Figs. 27C. That is, the fatigue crack initiation and propagation behaviors depend strongly on the spacing between two small pores and on the two pores with 90° or 45° tilted to the applied loading direction.
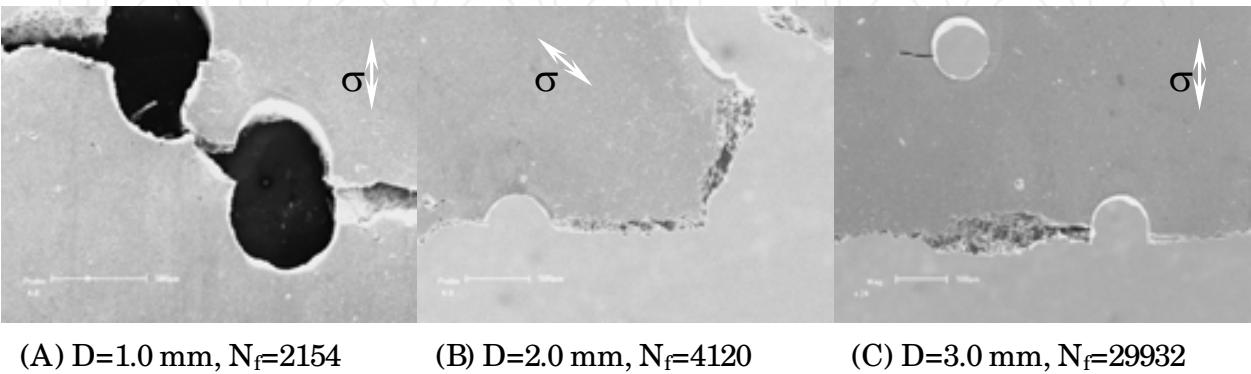

(A) D=1.0 mm, N_f=2154　　　(B) D=2.0 mm, N_f=4120　　　(C) D=3.0 mm, N_f=29932

Fig. 28. Cast AM60B alloy with the different spacing of 45° orientations at the two pores under σ_{max}=120MPa, R=0.1.

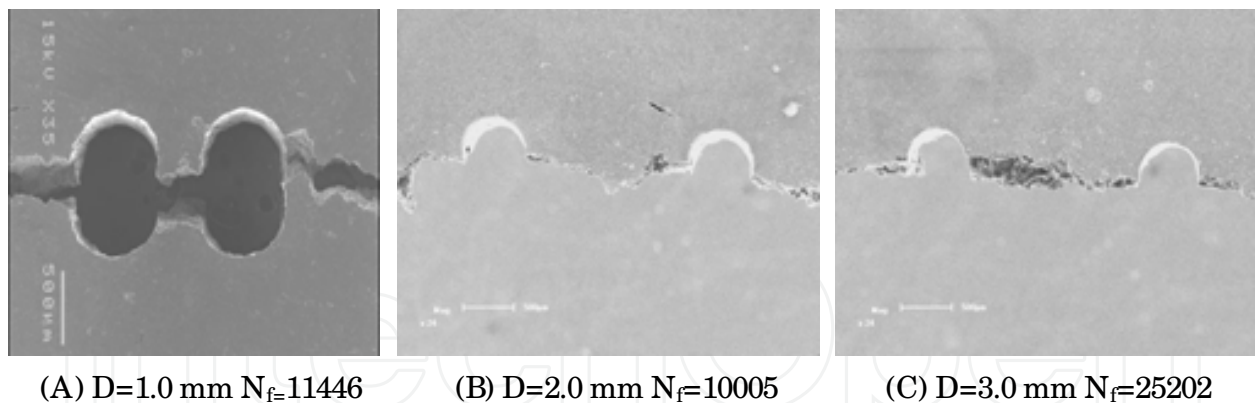(A) D=1.0 mm $N_{f=}$11446   (B) D=2.0 mm N_f=10005   (C) D=3.0 mm N_f=25202

Fig. 29. Cast AM60B alloy with the different spacing of 90° orientations at the two pores under σ_{max}=120MPa.

To validate the critical spacing value of two pores above mentioned 2.0 mm, Figs. 28 and Figs. 29 show the experimental evidences which are the effective results of different spacing and alignments of cast AM60B alloy under the same applied stress amplitude, respectively. For the specimens with the 45° orientations at the two pores as shown in Figs. 28, the effect of spacing between two pores on the fatigue fracture is obvious. In the Figs. 28C, the final fracture of specimen did not cause the coalescence of cracks at one pore with another pore when the spacing between two pores is over than 3.0 mm. But the spacing between two pores is less than 2.0 mm, the fatigue crack occurred at the two pores finally linked with each other. Therefore, we can obtain that the fatigue life increases with the increasing of spacing with the 45° orientation at the two pores. This reflects the fact that the interaction of fatigue cracks affects on the fatigue life. Likewise, when the alignment of two pores was changed as the 90° orientation as shown in Figs. 29, the experimental results indicated that the fatigue life of cast AM60B alloy is also affected by the spacing between two pores. And the critical value of spacing between two pores is approximate 2.0 mm. That is, when the spacing is over than 3.0 mm, the effect of alignment with two pores on the fatigue life of cast AM60B can ignore although there is slight difference in their fracture lives. One of reasons about this difference focus on the fatigue crack initiation life because of the quality of drilled pores. For example, the effect of the quality of drilled pores on the fatigue life of cast AZ91 alloy shown in Figs. 30. Although there are the same experimental conditions such as the spacing and alignment of two pores as well as under the applied stress level, the fatigue life exists in the slight difference after 5.25×10^4 cycles. This is because the fatigue crack initiation occurs preferentially at the rather bigger pore as shown in Figs. 30A. And if the fatigue crack occurs synchronously at the edges of two pores, the fatigue cracks cause easily a coalescence of cracks with another one, especially like as the rapidly linked cracks in the spacing between two pores as shown in Figs. 30B.

Alternatively, for 45° orientations at the two pores with the spacing (which is 1.5 mm, 2.0 mm, 3.0 mm, respectively) of cast AZ91 alloy, the fatigue life and fracture manners under the different applied stress amplitudes are respectively shown in Figs. 31. The fatigue cracks propagation path difference of cast AZ91 alloy with two pores specimens is very obvious. The interaction of fatigue cracks did not occur when the spacing is 3.0 mm.
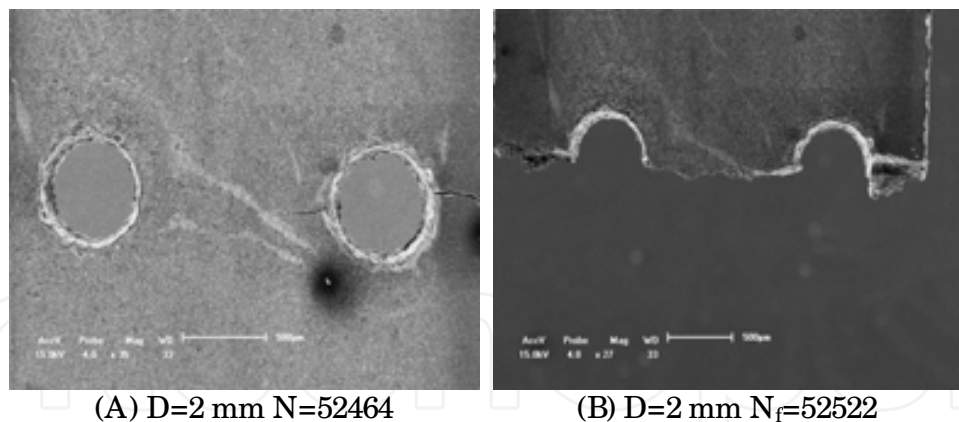
(A) D=2 mm N=52464   (B) D=2 mm N_f=52522

Fig. 30. Cast AZ91 alloy with the same spacing of 90° orientations at the two pores under σ_{max}=100 MPa.

(A) σ_{max}=170MPa, N_f=236   (B) σ_{max}=145MPa, N_f=952   (C) σ_{max}=123MPa, N_f=3924
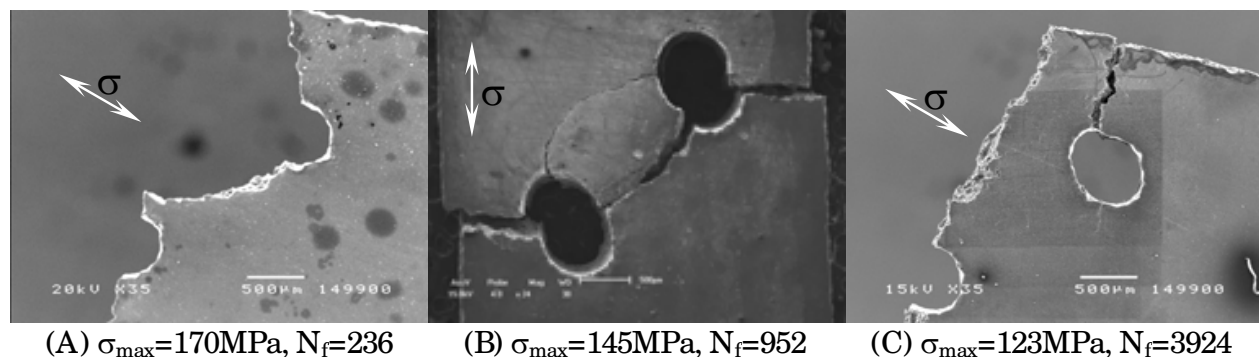
Fig. 31. Cast AZ91 alloy with the different spacing of 45° orientations at the two pores (1.5 mm, 2.0 mm, 3.0 mm)

For majority cast magnesium alloys, their fatigue lives are still dependence on the mechanical properties, especially the fracture toughness or elongation (%) of cast magnesium alloys. In general state, the greater of the fracture toughness or elongation (%) of cast magnesium alloys is, the longer their fatigue lives are as shown in Fig. 32. For example, the elongation of cast AM60B alloy is about 10% and the elongation of cast AZ91 alloy is about 3% so that the fatigue life of the former is longer than that of the latter under the same experimental conditions. This is because the brittle property of cast AZ91 alloy causes much easier multi-cracks initiation at the β-$Mg_{17}Al_{12}$ phase or interface both α-Mg grain and β-phase than that of cast AM60B alloy, alternatively the effect of smooth specimen and specimen with a notch on the fatigue life of cast AM50 alloy is also obvious, especially in the higher applied stress levels. However, when the cyclic numbers arrives at the 2×10^5, the effect of small notch on the fatigue life is gradually weaken because the notch of cast magnesium alloys depends mainly on the fatigue crack initiation life, which is to occupy a little part of total fatigue life of cast magnesium alloys under the lower stress levels. The investigations results indicated that the fatigue crack propagation life of cast AM50, cast AM60, AM60B and AZ91D alloys occupies approximately about 70%. Therefore, the high cyclic fatigue life of smooth specimen and specimen with a small notch has not almost difference under a low stress level as shown in Figs. 32. These curves indicated still that the relative fatigue life relation among cast magnesium alloys. These accurate relations of

fatigue live were validated by cast AM50, AM60, AM60B and AZ91. It is fact that the fatigue life of cast AZ91 alloy with a lower elongation is shorter than that of either cast AM60 alloy or cast AM50 alloy with a higher elongation under the same experimental conditions, especially in higher stress levels. Therefore, the fatigue property of cast AZ91 alloy (3%-elongation ratio) is weak to compare with cast AM60 alloy (7-10% elongation ratio) or cast AM50 alloy (9-11% elongation ratio). This is because the elongation ratio of material relates to the fracture toughness of material. The higher facture toughness of material is, the greater fatigue crack propagation resistance is.
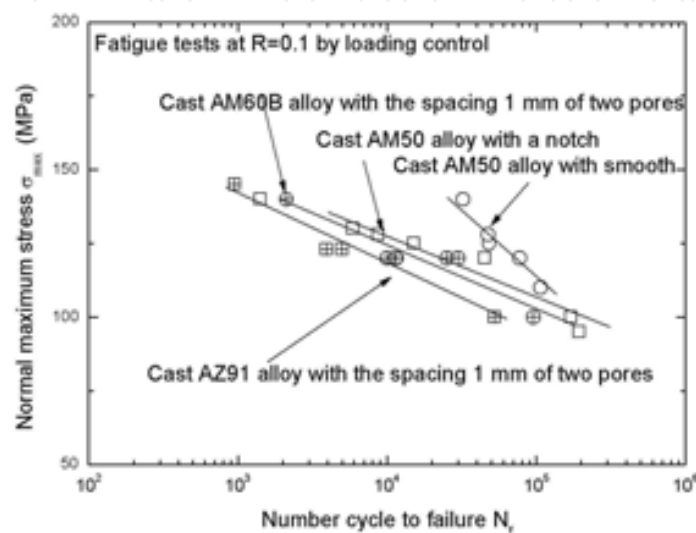
Fig. 32. *S-N* curves of cast magnesium alloys at the different conditions

3.2 Validation on the effect of two pores on the cracking behavior by optical displacement microscope

Above mentioned many results about the effects of spacing and orientations with the two pores on the fatigue cracking behavior of cast magnesium alloys, these results indicated that there is a critical spacing value of two pores with the 90° or 45° orientation whether to tack place the coalescence of crack at one pore with another one. To validate the critical value whether is correct and reliable, the tensile tests of cast AM60 alloy with 90° and 45° orientations of two pores were carried out by using the optical displacement microscope, which is usually stretched at a specific rate, and the force required that it is measured to cause an extension of a crack length $\delta\ell$. Force is measured by means of a load cell that is often a calibrated, stiff spring, and the extension is measured often by means of a device called an extensometer. All tensile tests used specimens have the approximate same pore diameter (D) of 0.68 mm and 4D (~2.72 mm) spacing. The tensile speed is about 10^{-3} mm/ min by the displacement control. These results indicated that there is obvious the stress concentration area evolutive process in prior to the crack initiation at the root of pores as shown in Figs. 33 and Figs. 34. When the applied strain value arrives at the 0.8% in prior to the yield stress as shown in Figs. 33B, the slight stress concentration region (see the white area) occurred at the root of each pore, and the stress concentration area mainly occupied at insider of two pores is greater than that at outsider of two pores as shown in Figs. 33C and 33D. With increasing the applied strain value of $\varepsilon = 3.0\%$, the stress concentration areas at the insider of two pores overlap gradually as shown in Figs. 33E so that the cracks easily

accelerate the crack growth in these regions. One clear crack was found in the plastic strain overlapped region when the applied strain value is about 3.7% as shown in Figs. 33F. The total evolutive process of stress/strain concentration on the surface of cast AM60 alloy agrees well with the experimental images based on the SEM *in-situ* observation of fatigue crack propagation tests as shown in Figs. 29.
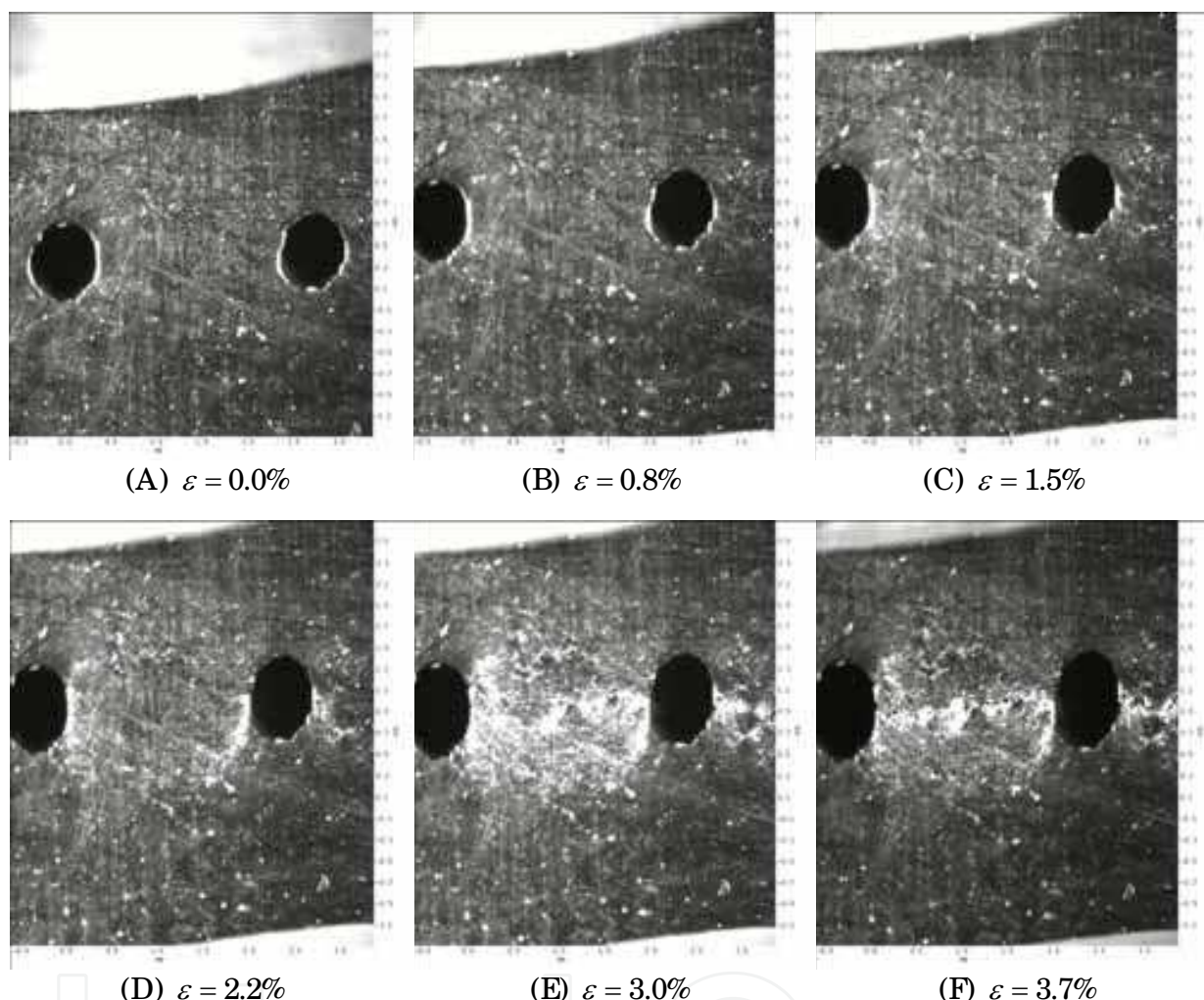

(A) $\varepsilon = 0.0\%$ (B) $\varepsilon = 0.8\%$ (C) $\varepsilon = 1.5\%$

(D) $\varepsilon = 2.2\%$ (E) $\varepsilon = 3.0\%$ (F) $\varepsilon = 3.7\%$

Fig. 33. Evolutive deformation process under the different strains for 90° orientations with the two pores.

As another typical tensile testing images of cast AM60 alloy specimen with two pores at a 45° orientations as shown in Figs. 34, the stress concentration region at the edges of two pores is different from above mentioned results as shown in Figs. 33, especially after the applied strain value being over than 2.0%. This means that the stress overlapped manner will influence on the fatigue crack propagation behavior according to the fracture mechanism of cast magnesium alloys. At the same time, you can see that the stress concentration diffusion process of cast magnesium alloy maybe result the multi-cracks. When the applied strain value increases to about 2.0-3.0% as shown in Figs. 34C and 34D, the stress concentration areas occur at much more overlapping or diffusion part. The crack propagation path has to deflect to the overlapping regions as shown in Figs. 34E and 34F. In addition, the cracks initiation and propagation result the release of stress

concentration compared with the change of white regions in both Figs. 34D and 34E. Compared with the results as shown in Figs. 33 and Figs. 34, the effect of two pores orientations on the evolutive process of the stress concentration or on the crack propagation path can be not ignored. The visible tensile and fatigue cracks of cast AM60 alloy occur almost at the root of any pore under the different orientations of two pores. Therefore, the effect of two pores orientations on the crack initiation behavior is rather slight. For example, the crack initiation of cast AM60 specimen with either 90° or 45° orientations occur at the root of any pore when the applied strain is about 3.7% and 4.0%, respectively. However, the effect of orientations of two pores on the strength or fatigue life of cast AM60 alloy can be not ignored. This means that this effect mainly focus on the crack propagation behavior of cast magnesium alloys.

| (A) $\varepsilon = 0.0\%$ | (B) $\varepsilon = 1.0\%$ | (C) $\varepsilon = 2.0\%$ |
| (D) $\varepsilon = 3.0\%$ | (E) $\varepsilon = 4.0\%$ | (F) $\varepsilon = 5.0\%$ |
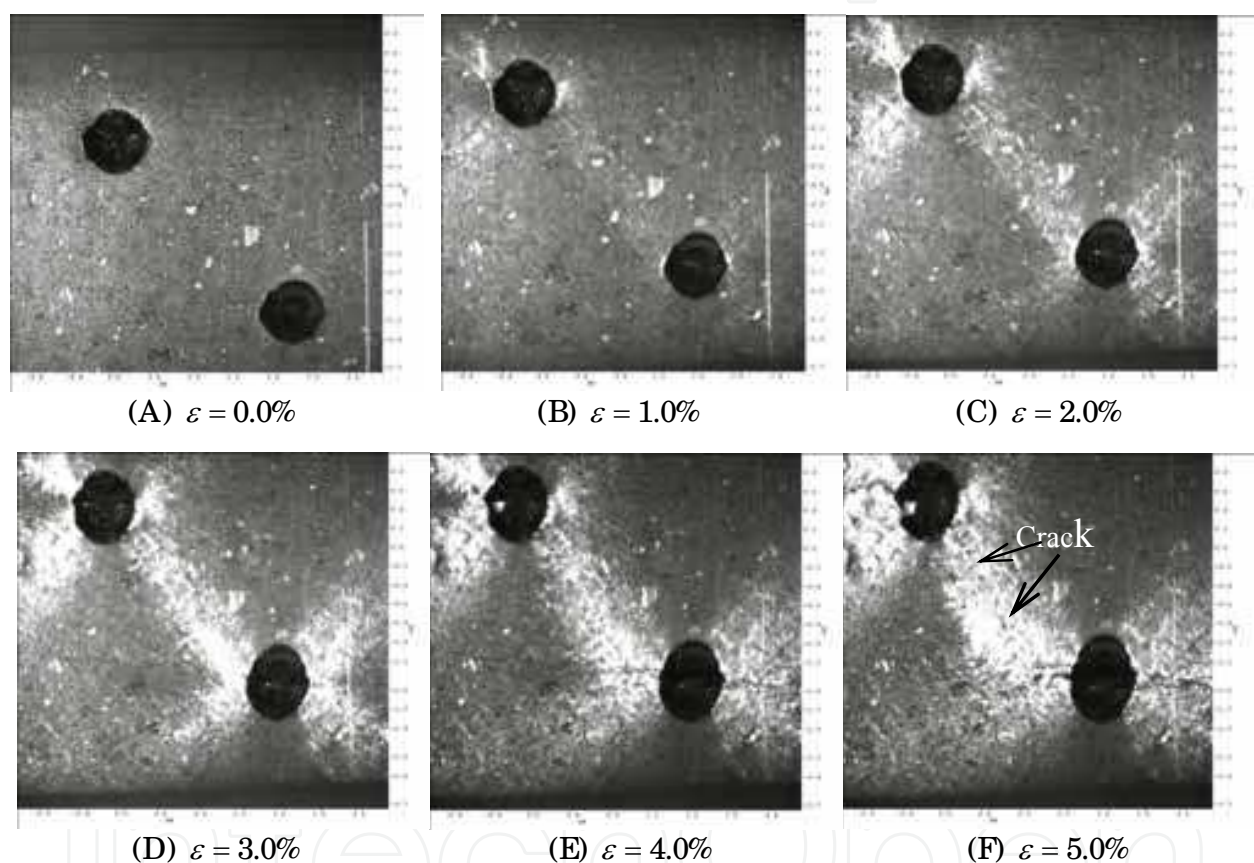
Fig. 34. Evolutive process of plastic deformation under the different strain levels for 45° orientations with the two pores.

To validate the effect of different orientations on the fracture strength of cast AM60 alloy, we give the stress-strain curves of cast AM60 specimens with different orientations of two pores as shown in Figs. 35. These pores can be defined as an initial crack or defect. These results indicated that the effect of different orientations on the fracture strength and fracture toughness of cast AM60 alloy under the static tensile loading is obvious. That is, the fracture strength and toughness of a specimen with 90° orientations are lower than that of a specimen with 45° orientations. This means that the former damages or fractures prior to the latter. As the engineering stress as shown in Fig. 35, the original and strained dimensions are related through $A_0 \ell_0 = A_i \ell_i$, where A_0, ℓ_0 are the original transverse cross-sectional area

and sample gage length, respectively, and A_i, ℓ_i represent these quantities in the strained condition. As the cross-sectional area decreases with increasing strain, the sample experiences an effective stress greater than that suggested via calculation of stress based on the initial cross-sectional area. We can define an engineering stress as following:

$$\sigma = \frac{F}{A_0} \qquad (4\text{-}8)$$

When the tensile test of cast magnesium alloy is at low strains, the deference between A_0 and A_i can be ignored. Therefore, based on the stress-strain curves in Fig. 35, the effect of cast AM60 alloy with the different orientations of two pores on the tensile properties can be described by the difference between both curves. For example, when the strain value is closed to the 3.0% value, the plastic flow in both curves presents the different stress concentrated characteristics due there is an effect of stress concentrated overlapping region fraction. With increasing the overlapping region fraction, the failure resistance of sample becomes smaller and smaller. On the other hand, the failure possibility of sample with a 90° orientations of two pores is greater than that of sample with a 45° orientations of two pores at the same spacing. The phenomenon is an evidence of a "working softening" effect of material in the stress concentrated overlapping area compared with the images as shown in Figs. 33E and Figs. 34D. At the same time, we can deduce that this is why the fatigue life of a specimen with 90° orientations is lower than that of a specimen with 45° orientations when the spacing of two pores is not over than 2.0 mm above mentioned.
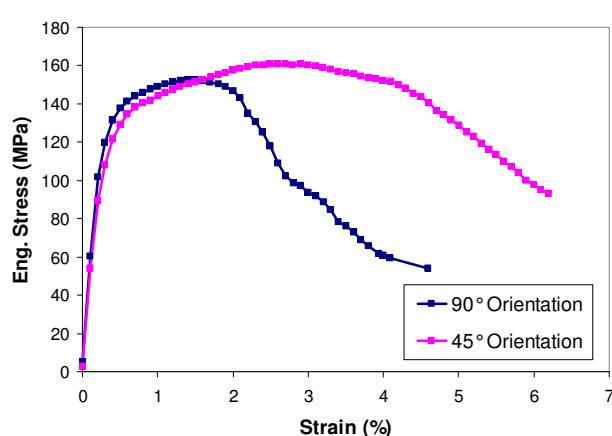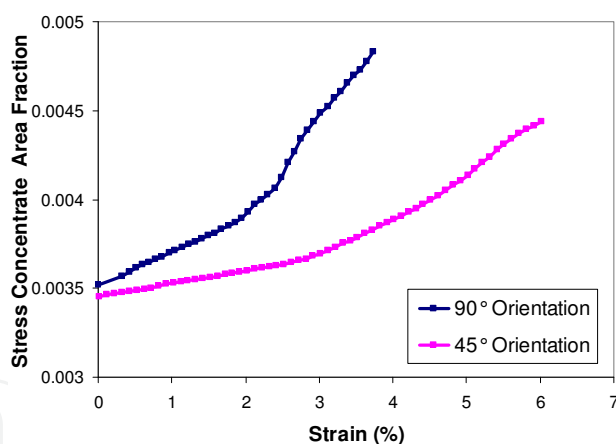

Fig. 35. Stress-strain curves   Fig. 36. Stress concentrate diffusion curves

Alternatively, to compare with the difference between the effects of different orientations on the damage of cast magnesium alloys, the relationship curves between the stress concentrated areas near the different orientations of two pores and the applied strain (%) were plotted in Fig. 36. It is clearly seen that the curves of the stress concentrated area fraction versus the applied strain indicates the effect of 90° orientations on the fracture of cast magnesium alloy is much obvious than that of 45° orientations at the same spacing. That is, the stress concentrated overlapping region or diffusion area with 90° orientations of two pores is greater than that with 45° orientations of two pores under the same strain level as shown in Fig. 36. This means that the former easily cause the crack initiation and propagation at these regions because of the theory of fracture mechanics of materials.

Especially it is much obvious for the effect of orientation on the stress concentrated degree when the applied strain value is over than 3%. At the same time, these results validated effectively that the effects of two pores' spacing and orientation on the fatigue crack initiation and propagation behavior are correct based on SEM *in-situ* observations.

3.3 Modeling on two pores of cast magnesium alloy

There are several interesting aspects of the critical fracture condition when we consider the effect of two pores with the different spaces and orientations on the failure of cast magnesium alloys. One is that the yield strength and cracking criterion are the same tension as in fatigue of cast magnesium alloys. As mentioned, when the local stress ahead of a crack tip exceeds a critical strength value of cast magnesium alloy, the crack will cause to failure of material. In majority states, the von Mises yield stress can be as the failure criterion value. It is expressed as

$$\sigma_{Miese} = \sqrt{[(\sigma_1 - \sigma_2)^2 + (\sigma_2 - \sigma_3)^2 + (\sigma_3 - \sigma_1)^2]/\ 2} \qquad (4\text{-}9)$$

The condition states that yielding will not take place for principal stress combination such that the von Mises stress (σ_{Miese}) near the pores is less than the yield stress of cast magnesium alloy, but that flow will occur if it is greater than the yield stress. Due to the presence of small pore in the plate, the stress states around a pore will cause the stress concentration, stress states transmitted by each other and the cumulative evolvement of plastic strain in the fatigue process of materials. In general condition, we can use the von Mises stress replaces to the uniaxial tensile stress. In fact, the fracture or failure of materials depends strongly on the state of stress. This is why there are the different crack propagation characteristics of the same cast magnesium alloy with different two pores' spaces and orientations in the experimental results.

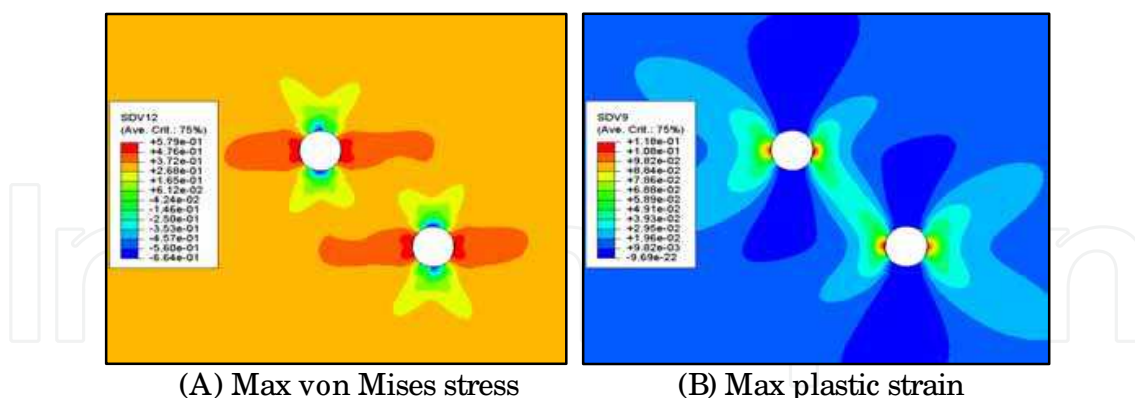(A) Max von Mises stress   (B) Max plastic strain

Fig. 37. von Mises stress and plastic strain distributions around the two pores

To validate the evolutive process of stress concentration region closed to the two pores, we simulated the von Mises stress and maximum plastic strain distributions closed to the two pores. These von Mises stress and plastic strain distributions around the two pores can tell quantitatively us the crack initiation and crack propagation path of material as shown in Figs. 37. The contour plots of stress triaxiality and effective plastic strain at about 2% indicated that the von Mises stress evolutive direction is approximate 90° tilted the applied loading direction, which it causes the main reason of crack initiation as shown in Figs. 37A.

All SEM *in-situ* observations results about fatigue crack propagation tests and tensile tests of cast magnesium alloys with different orientations and spaces of two spherical pores have validated that the crack occurred mainly at the root of pore and the early stage of crack propagation direction was along 90° tilted to the applied loading direction. This means the crack initiation behavior depends strongly on the maximum strength theory of cast magnesium alloys as shown in Figs. 37A. However, with increasing the applied stress level, the strain (plastic strain) value round the two pores is also to increase nonlinearly (to meet with the Ramberg-Osgood model [42]) based on the constitutive equations of cast magnesium alloys as shown in Figs. 37B. Therefore, the crack propagation behavior of cast magnesium alloys with the different orientations and spaces of two pores depends strongly on the overlapping degree of stress concentration or plastic strain, which dominates the macroscopical crack propagation direction of cast magnesium alloys. At the same time, the overlapping degree of stress concentration or plastic strain will cause the fracture mode to transfer from mode I fracture to mode I/ II fracture. That is, the shear stress comes from the plastic strain in local area, especially in the overlapping region based on the interaction of stress concentration area around the two pores. For example, when the crack initiation occurs at the root of pore as a sketch map shown in Fig. 38, the stress at crack tip in the mark "•" can be expressed as following:

$$\sigma_\theta = \frac{C_0}{\sqrt{2\pi r}}[K_I(C_1 - \cos\theta)\cos\frac{\theta}{2} + K_{II}(3\cos\theta + C_2)\sin\frac{\theta}{2}]$$

$$C_0 = \frac{-2\alpha(1-\nu)}{1+3\alpha-4\nu\alpha}, C_1 = \frac{-2(1+\nu-2\alpha\nu)}{1+\alpha-2\nu}, C_2 = \frac{2(1+2\alpha((1-\nu))}{1+3\alpha-2\nu}$$

(4-10)

Where K_I, K_{II} denote the stress intensity factor of mode I and mode II fractures, respectively. α denotes the modulus ratio of inhomogeneous materials or the inhomogeneous phases. When $\alpha = 1$, corresponding to homogeneous material, Eq. (4-10) reduces to the well known result of a mix mode I/ II fracture of material:

$$\sigma_\theta = \frac{C_0}{2\sqrt{2\pi r}}[K_I(1+\cos\theta) - 3K_{II}\sin\theta]\cos\frac{\theta}{2}$$
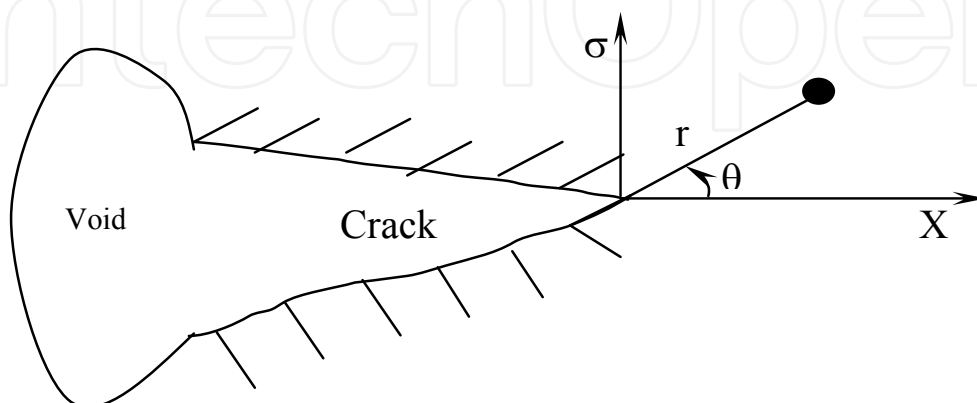
(4-11)

Fig. 38. A mixed fracture mode in the crack tip

From the solution Eq. (4-10) obtained, the angle of maximum tangential stress θ_f can be determined by using $\partial\sigma_\theta / \partial\theta = 0$ and $\partial\sigma_\theta / \partial\theta < 0$. An 'eligible' interface or boundary, at which the $\sigma_{\theta\max} \geq \sigma_f$ (σ_f is the fracture stress of the interface or boundary) is satisfied, will be located at the interface or boundary of cast magnesium alloy. Then the critical stress intensity factor, or the apparent fracture toughness of the cast magnesium alloy, can be established. The crack growth path deflecting main reason should be by local plastic strain to occur compared with the results as shown in Figs. 37 and Fig. 38. The factors such as the elevated temperature and pores with different spacing and orientations are one of main reasons to affect on the local plastic distribution when the same applied stress.

4. Effects of testing conditions on fatigue life of cast magnesium alloys

Above mentioned fatigue life of typical cast magnesium alloys as shown in Fig. 32, these results involve that the effects of samples with a single side notch and with two pores at different orientations, spaces and vacuum states on the fatigue life can be not ignored. However, it is difficult to distinguish that the fatigue lives of cast magnesium alloys are how to be affected by these testing conditions even if we known that the fatigue damage mechanism and fatigue crack growth rate at the different conditions of cast magnesium alloys.

As majority cast magnesium alloys, the fatigue life can be divided into two parts: fatigue crack initial life and fatigue crack propagation life. The fatigue crack propagation life can be estimated by the fatigue crack growth rate such as Eq. (4-1) and the fatigue crack initial life has to be deduced based on the *S-N* curves of smooth samples or to do some fatigue tests with smooth samples at the minimal measurable length of fatigue crack initiation although it is rather difficult work. Therefore, many investigators focused on how to obtain the fatigue crack growth rate or *S-N* curves of materials at the different conditions by the experimental manners. Especially, when the fatigue crack propagation life of majority metals occupies about over than 70% of total fatigue life, it is very important for the fatigue crack propagation tests of materials, which brings significant advantages in estimation the fatigue life of cast magnesium alloys or a design of automotive and aircraft components. The fatigue crack propagation process is more important in service for most ductile materials because the fatigue life is mainly determined by the cycles spent, especially spent for the cycles of the small crack growth [49,50]. With the development of techniques in a microscopy, it is possible to accurately and directly measure the length of fatigue small cracks growing. Examples of this are *in-situ* observations with SEM that allow us to investigate the fatigue crack initiation and propagation of metals [51].

4.1 Effect of elevated temperatures on the fatigue life

Fig. 39 shows that the *S-N* curves of cast AM50 samples with a notch (the radius of notch is about 50 μm in these *S-N* curves) were carried out at different temperatures in a vacuum chamber. With increasing the elevated temperature, the fatigue life of the cast AM50 magnesium alloy decreased monotonously. This means the fatigue life of cast AM50 Mg alloy depended mainly on the fatigue crack growth rate at these temperatures. Viewing the fatigue failure patterns at elevated temperatures (more than 100 °C) when the applied stress
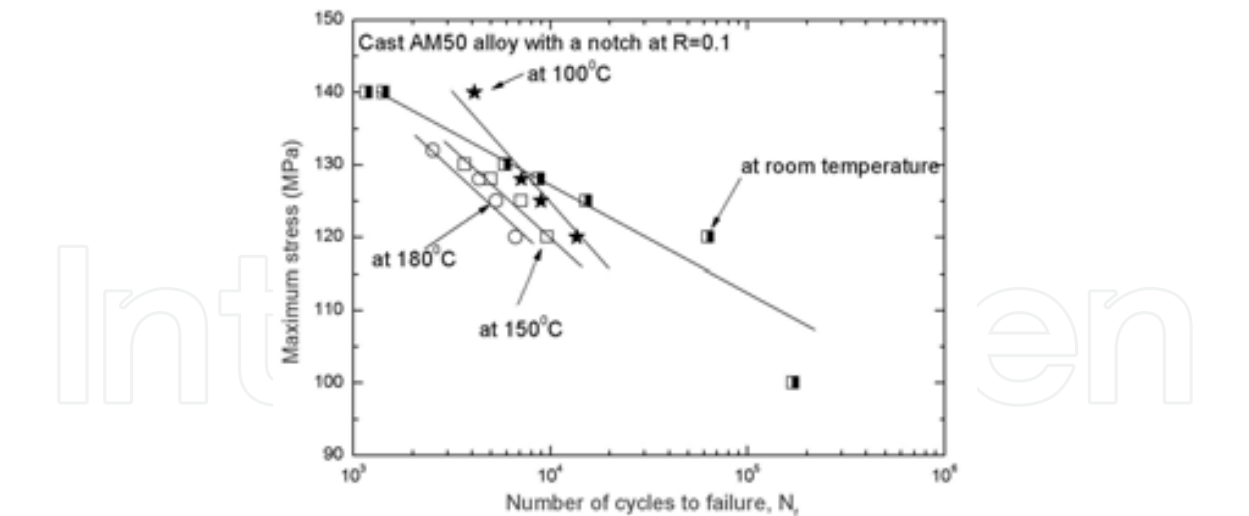
Fig. 39. *S-N* curves at different elevated temperatures of cast AM50 alloy

amplitude is a constant, it is found that the fatigue failure mechanism is mainly cleavage fracture of α-Mg grains and Mg-dendrites as shown in Figs. 40A (It can be classified as the Mode I crack.). This cleavage fracture is produced by repeated cycling on the crack tip plastic zone. Fatigue small cracks in vacuum chamber were accelerated with the increasing thermal-mechanical loading because the β-phase ($Mg_{17}Al_{12}$) in cast AM50 magnesium alloy began to soften at the high temperature. Compared with properties of fatigue cracks propagated at different temperatures in a vacuum chamber indicated that the propagation of fatigue small cracks mainly along the interdendrite region or along the boundary of α-Mg grains at the room temperature [14,15] and the fatigue small cracks propagated passing through inside of the Mg grains because these regions were soften at higher temperatures. As shown in Figs. 40B, there are some significant plastic slip vestiges which appeared on the up and down of the crack tip and lied at about 45° inclined with respect to the crack, so that the growth rate of small fatigue cracks at higher temperatures is larger than that at room temperature in a vacuum chamber. The fatigue small crack path is clear in Figs. 40C and Figs. 40D either cleft the α-Mg grains or passed along the boundary of the α-Mg grains. The former (transgranular fracture) was occurred more frequently than the latter at the high temperatures. Our observation results indicated that the small fatigue cracks preferentially grew in a Mode I direction. Microstructural small cracks, however, frequently deviate in order to avoid an obstacle or to link with a weakened material zone. Gall et al. have also
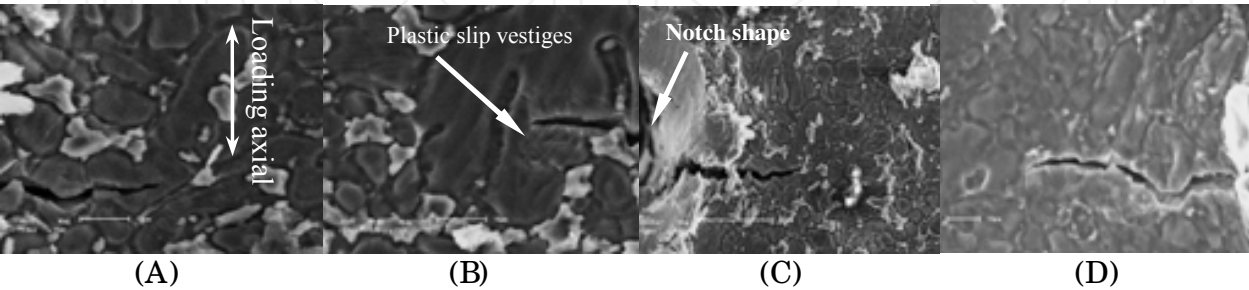

Fig. 40. SEM images of fatigue crack growth under different loadings at R=0.1. (A) σ_{max}=128 MPa, T=150°C, N=4109; (B) σ_{max}=125 MPa, T=150°C, N=5819; (C) σ_{max}=128 MPa, T=150°C, N=4260; (D) σ_{max}=120 MPa, T=180°C, N=12526.

obtained a similar conclusion for AM60B specimens tested in vapor environment [30]. Thus, the propagation rates of small fatigue cracks of Mg-Al alloys are strongly dependent on the temperatures.

4.2 Effect of notch and oxidation on the fatigue life

To observe fatigue small crack initiation and propagation process, a notch in the edge of specimens were cut manually. As the typical case, the notch radius and depth of all notch specimens are approximately 50 μm, 100 μm, respectively. The fatigue tests with the smooth specimens of cast AM50 Mg alloy were also carried out to compare the difference between fatigue life of smooth and notched specimens either in the vacuum or in air. The corresponding *S-N* curves are shown in Fig. 41. It is clearly shown that the difference of these influences are greater under the higher stress level than under lower stress level, whether or not the environment is air or vacuum. On the other hand, this means that the effect of the notch on the fatigue life became rather obvious with increasing stress level. It is confirmed that the notch size mainly affects the fatigue initiation life of material.
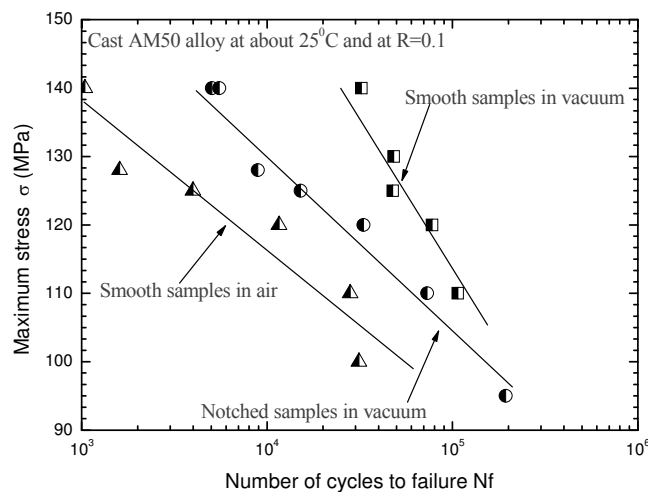

Fig. 41. Effect of notch and oxidation on *S-N* curves of cast AM50 alloy

The maximum von Mises stress value in the stress concentration region around the notch tip increases with the applied stress increasing. If the stress level in the stress concentration region reaches a certain magnitude such as over than 70% yield stress of cast magnesium alloy, the fatigue crack will occur in the stress concentration region after a several hundreds cycles. However, at the lower stress level such as less than 60% yield stress of cast AM50 alloy, the differences of the total fatigue lives of specimens with a notch and smooth are mainly contributed by the fatigue crack initiation life, which is controlled by stress concentration degree such as it refers to two parameters both different radiuses and depths of a notch. For example, this effect was reported that the number of cycles spent on fatigue crack initiation is less than one half of the total fatigue life for smooth specimens of the general metals [52]. Therefore, the effect of a notch on the fatigue life of cast magnesium alloys is similar to the reported results in Literature [52].

In addition, cast Mg alloys have generally a low oxidation resistance, thus there is a difference about fatigue life of cast magnesium alloys under different fatigue tests. For example, the two *S-N* curves of cast AM50 alloy indicates that the fatigue life in air is shorter than that in vacuum under the same stress amplitude as shown in Fig. 41. This means that

the effect of air corrosion on the fatigue of this alloy is not ignored, especially in an absence of surface barriers on cast magnesium alloys, e.g. in the case without oxide films or anodized coating [30,52]. At the same time, the *S-N* curves indicated still that environmental effect both in air and vacuum on the fatigue life of cast magnesium alloy has the different trends at low and high stress levels. At the lower stress level, the effect of environmental effect both in air and vacuum becomes smaller and smaller, contrarily larger and larger at higher stress level for the smooth specimens.

4.3 Effect of cast magnesium alloys on the fatigue life

As cast magnesium alloys, the mechanical properties (especially the elongation (%) or fracture toughness) differ observably from each other, such as cast AM50 alloy and cast AZ91 alloy. Therefore, the fatigue crack initiation life of these materials is observably different. For example, Fig. 42 shows the fatigue curves of cast AM60 and AZ91 alloys at the different fatigue crack initiation and propagation tests. Due the fatigue tests are LCF, the fatigue life of cast magnesium alloys depends on the plastic strain energy so that the elongation ($\delta\%$) (or fracture toughness) of cast magnesium alloy dominates its fatigue life. The many fatigue cracks for quasi-brittle secondary phase in the cast magnesium alloy occur easily at their interface or boundary as shown in Figs. 43A. At the same time, the plastic
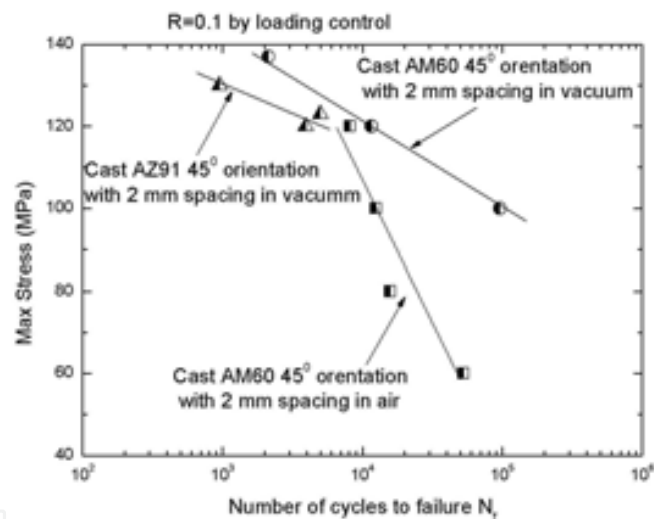

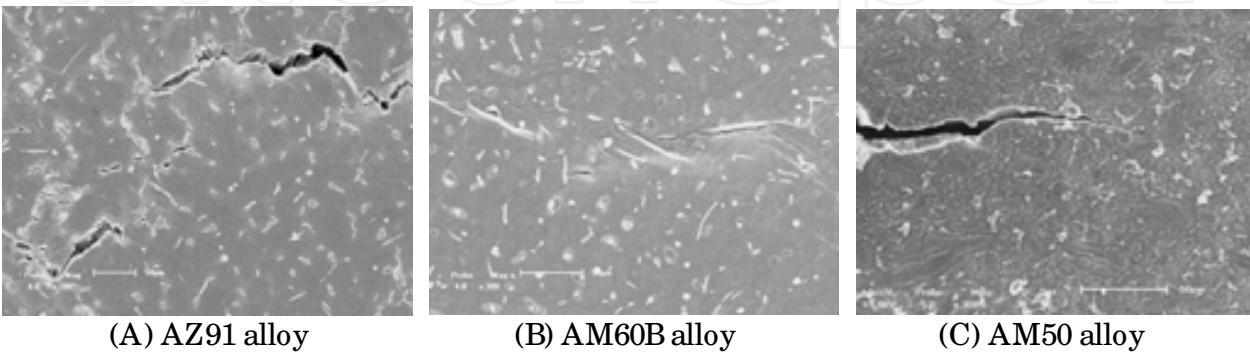Fig. 42. Effect of environmental vacuum and magnesium alloys on *S-N* curves.

(A) AZ91 alloy   (B) AM60B alloy   (C) AM50 alloy

Fig. 43. Fatigue crack characteristics of different cast magnesium alloys

deformation will present at rather softness α-Mg phase near the fatigue crack as shown in Figs. 43B. Therefore, the fatigue propagation life of multi-cracks is rather shorter than that of single fatigue crack because there is combined near these cracks so that it causes to accelerate the fatigue crack growth rate of cast magnesium alloy. For the fatigue life of cast AM60 alloy in air and vacuum conditions, the differences both conditions can be not ignored as shown in Fig. 42.

5. Summary

Fatigue refers to mechanical failure (and the processes leading to it) when a cast magnesium alloy is subjected to a cyclical stress or strain amplitude that would not result in fracture during monotonic loading. This kind loading can take place in all classes of materials. However, it was not commonly thought to happen in a quasi-brittle cast magnesium alloy, for small cracks formed during fatigue of quasi-brittle cast magnesium alloy quickly lead to catastrophic fracture owing to the low fracture toughnesses of majority cast magnesium alloys. As a result, fatigue small crack initiation and propagation behavior, and relative several central issues dealing with the effects of some factors (temperature, notch and pores etc.) on the fatigue cracking behaviors and life of cast magnesium alloys (including AZ91D, AZ91, AM60B, AM60 and AM50) were investigated by the different experimental methods. The fatigue cracking behavior, fatigue life of cast magnesium alloys and the influencing factors were detailedly discussed in this chapter.

The fatigue crack initiation behavior (Stage I of the fatigue process) of cast magnesium alloys are formed initially at surface flaws and/ or defects (including to the manual notch) that promote localized flow in their vicinity. Less frequently they nucleate at internal inhomogeneities (e.g., interdendritic pore, pores, secondary phase particles etc.) that likewise serve to promote stress concentrations region in the cast magnesium alloys surrounding them. These types of fatigue nucleation events are common to metals. This leads to the development of a feature that, at some stage, can be characterized as a Stage I crack as shown in Figs. 9B. In the initial growth of such, it propagates in a direction determined by slip crystallography, and this direction is not normal to the principal stress axis. Thus, Stage I crack propagation is defined by a flow, rather than a fracture, criterion. After such a crack has progressed a certain distance, it alters its direction so that it becomes normal to the principal stress axis or applied loading direction. At this point further advance depends on other factors similar to those applying to tensile fracture as shown at the 3.2 section in this chapter. However, the effects of rather smaller radius of notch and the different spacing and orientations of two pores can be not ignored.

Following this alteration of its course in micro scale, continued propagation of the crack takes place in an intermittent manner (the crack growth region, Stage II of fatigue). The crack growth rate, $d\ell / dN$ (the change in crack length ℓ, with the number of cycles, N) is related to the "either a term of $\sigma_{\max}^n \ell$ at R=0.1 (or $\Delta\sigma^n \ell$ at R=-1). The higher the value of $\sigma_{\max}^n \ell$ or ΔK, the greater of $d\ell / dN$ is, and $d\ell / dN$ of a given cast magnesium is uniquely related to the term of $\sigma_{\max}^n \ell$ or ΔK. For most cast magnesium alloys there exists a threshold cyclical stress intensity, ΔK_{th} below which fatigue cracks will not propagate. Sometimes, if the fatigue crack growth rate is rather lower than the given value, such as the rate of about 10^{-10} m/ cycle, it can be defined as the threshold value of fatigue crack growth rate. Using the cast magnesium alloys at ΔK values less than ΔK_{th} constitutes "fail-safe" fatigue-fracture design. Unfortunately, ΔK_{th} is usually quite low, so that use of it in design constitutes inefficient cast

magnesium alloys utilization. Consequently, fatigue design philosophy assumes the presence of fatigue cracks that will grow during service, but also employs empirical guidelines coupled with timely service inspection to see to it that such cracks do not progress to the extent that cast magnesium alloys failure occur during the intended service life. As understanding the fatigue cracking mechanism and fatigue crack growth rate of cast magnesium alloys at the certain condition, the residual life of cast magnesium alloy can be estimated by continuously detecting the measurable fatigue crack propagation length.

For most cast magnesium alloys are best suited to LCF application. This is related to the fact that the Stage II growth occupies most of the material's life during low-cycle fatigue. It is clear that hard, quasi-brittle cast magnesium alloys do not resist crack advance.

Temperature has an influence on fatigue response of cast magnesium alloys. This is important for evaluated temperature of cast magnesium alloys influence on the fatigue crack propagation mechanism. For example, the fatigue crack initiation of cast AM50 alloy occurred at the root of notch (when the radius of notch is less than the 50 μm) but the early stage of crack propagation is along either the boundary of α-Mg grain or to cleave the α-Mg grain in front to the crack tip. The fatigue crack propagation mechanism in the microscopically zone is analogous to the quasi-brittle or quasi-ductile (intervenient brittle and ductile) fracture mechanism of engineering alloys. At RT, we did not find that the α-Mg grain of cast AM50 alloy was cleaved. When the elevated temperature is over than 100 °C, the fatigue crack propagation is also either along the boundary of α-Mg grain or to cleave the α-Mg grain. In addition, the fatigue crack propagation mechanism of cast AM50 alloy at the elevated temperature indicated that the branch fatigue crack was found as shown in Figs. 13B. This means that the fracture mechanism of cast magnesium alloy at the elevated temperature which is Mode I and Mode II differs obviously from that which is only Mode I at room temperature in microscopically zone. Corresponding effect of the elevated temperatures on the fatigue cracking mechanism of cast magnesium alloys has analogous to composite fractures of Mode I/ II. Therefore, the effect of the elevated temperature on the fatigue crack propagation mechanism of cast magnesium alloys can be not ignored. This is because the elevated temperature easily causes the β-$Mg_{17}Al_{12}$ becomes a softness so that the deformation mismatch between the α-Mg grain and β-$Mg_{17}Al_{12}$ phase becomes weak at the elevated temperatures. This is a competitive result of the interface strength and the fracture strength of α-Mg grain.

Small pores or radius of notch has an influence on the fatigue crack propagation behavior of cast magnesium alloys, which involves the FE calculation for the stress/ strain distribution around each pore. All calculated von Mises stresses can be scaled with respect to magnitude of the applied stress or transmit strain based on the constitutive equations of cast magnesium alloys. The stress distribution will be illustrated by the principal stress and the von Mises effective stress on crack propagation plane around the pore. It is approximately equivalent to the axial stress and vanishes at the pole and takes its largest values at the overlap region of plastic deformation of cast magnesium alloy.

As the effects of spacing and orientations with two pores on the fatigue cracking behavior of cast magnesium alloys, these experimental results indicated that there is a critical spacing value of two pores with the 90° or 45° orientations whether to tack place the coalescence of crack at one pore with another one, which is about 2.0 mm either 90° or 45° orientations with two pores. The effect of different orientations on the fracture strength and fracture toughness of cast AM60 alloy under the static tensile loading is obvious. That is, the fracture strength and fracture toughness of a specimen with 90° orientations are lower than that of a

specimen with 45° orientations. This means that the former damages or fractures prior to the latter. These experimental conclusions can be validated and explained by the difference of stress concentration area fraction as shown in Fig. 36.

Cast magnesium alloys have generally a low oxidation resistance, thus there is a difference about fatigue life of smooth and notch specimens under different fatigue tests. For example, the two S-N curves of cast AM50 Mg alloy indicates that the fatigue life in air is shorter than that in vacuum under the same stress amplitude as shown in Fig. 41. This means that the effect of air corrosion on the fatigue life of this alloy is not to be ignored, especially in an absence of surface barriers on cast magnesium alloys, e.g. in the case without oxide films or anodized coating [30,52]. At the same time, the S-N curves indicated still that environmental effect both in air and vacuum on the fatigue life of cast magnesium alloy has the different trends at low and high stress levels. At the lower stress level, the effect of environmental effect both in air and vacuum states becomes smaller and smaller, contrarily larger and larger at the higher stress level for the smooth specimens as shown in Fig. 41.

6. Acknowledgement

7. References

[1] Mordike BL, Ebert T. Magnesium properties-applications-potential. Mater Sci Eng A 2001; 302: 37-45.

[2] Sakkinen DJ. Physical metallurgy of magnesium die cast alloys. SAE Technical Paper 940779, Detroit (MI): SAE; 1994.

[3] Mayer H, Papakyriacou M, Zettle B, Stanzl-Tschegg SE. Influence of porosity on the fatigue limit of die cast magnesium and aluminium alloys. Int J Fatigue 2003; 25: 245-256.

[4] Kadiri Haitham EI, Xue YB, Horstemeyer MF, Jordon JB, Wang PT. Identification and modeling of fatigue crack growth mechanisms in a die-cast AM50 magnesium alloy. Acta Mater 2006; 54: 5061-5076.

[5] Horstemeyer MF, Yang N, Gall K, McDowell DL, Fan J, Gullett PM. High cycle fatigue of a die cast AZ91E-T4 magnesium alloy. Acta Mater 2004; 52: 1327-1336.

[6] Gall K, Biallas G, Maiers HJ, Horstemeyer MF, McDowell DL. Environmentally influenced microstructurally small fatigue crack growth in cast magnesium. Mater Sci Eng A 2005; 396: 143-154

[7] Shih TS, Liu WS, Chen YJ. Fatigue of as-extruded AZ61A magnesium alloy. Mater Sci Eng A 2002; 325: 152-162.

[8] Biallas G and Maier HJ. In-situ fatigue in an environmental scanning electron microscope-potential and current limitations. Int J Fatigue 2007; 29: 1413-1425.

[9] Tang B, Li SS, Wang XS, Zeng DB. An investigation on hot-crack mechanism of Ca addition into AZ91D alloy. J Mate Sci 2005; 40(11): 2931-2936.

[10] Tang B, Wang XS, Li SS, Zeng DB. Effects of Ca combined with Sr additions on microstructure and mechanical properties of AZ91D magnesium alloy. J Mate Sci & Tech 2005; 21(5):574-578.

[11] Tang B, Li SS, Wang XS, Zeng DB, Wu R. Effect of Ca/ Sr composite addition into AZ91D alloy on hot-crack mechanism. Scripta Mater 2005; 53(9):1077-1082.

[12] Kim KC, Nam SW. Effects of Mn-dispersoids on the fatigue mechanism in an Al-Zn-Mg alloy. Mater Sci Eng A 1998; 244(2): 257-262.

[13] Wang XS, Jin L, Li Y, Guo XW. Effect of equal channel angular extrusion process on deformation behaviors of Mg-3Al-Zn alloy. Mater Lett 2008; 62:1856-1858.

[14] Wang XS, Lu X, Wang HD. Investigation of surface fatigue microcrack growth behavior of cast Mg-Al alloy. Mater Sci Eng A 2004; 364: 11-16.

[15] Wang XS, Fan JH. SEM online investigation of fatigue crack initiation and propagation in notched cast magnesium specimens. J Mate Sci 2004; 39(7): 2617-2620.

[16] Wang XS, Fan JH. An evaluation the growth rate of small fatigue cracks in cast AM50 magnesium alloy at different temperature in vacuum environment. Int J Fatigue 2006; 28(1): 79-86.

[17] Wang XS, Liang F, Fan JH, Zhang FH. Investigations on low-cycle fatigue small crack initiation and propagation mechanism of cast magnesium alloys based on in-situ observation with SEM. Philos Mag 2006; 86(11):1581-1596.

[18] Wang XS, Fan JH. Growth rate of small fatigue cracks of magnesium alloy at different conditions. Mater Sci Forum 2007; 546-549: 77-80.

[19] Fouret C, Degallaix S. Experimental and numerical study of the low-cycle fatigue behavior of a cast metal matrix composite Al-SiCp. Int J Fatigue 2002; 24(2-4): 223-232.

[20] Blochwitz C, Tirschler W. In-situ scanning electron microscope observations of the deformation behaviour of short cracks. Mater Sci Eng A 2000; 276(1-2):273-276.

[21] Andersson H, Persson C. In-situ SEM study of fatigue crack growth behaviour in IN718. Int J Fatigue 2004; 26(3):211-219.

[22] Marx M, Vehoff H. Propagation of microcracks in single crystalline nickel-based superalloys: size effects on the crack opening. Mater Sci Eng A 2004; 387-389: 511-515.

[23] Gilbert CJ, Ritchie RO. On the quantification of bridging tractions during subcritical crack growth under monotonic and cyclic fatigue loading in a grain-bridging silicon carbide ceramic. Acta Mater 1998; 46(2): 609-616.

[24] Tanaka Y, Deng ZY, Liu YF, Masuda C. In situ observation on fatigue crack growth in SCS-6/ Ti-15-3 composite at elevated temperatures. Acta Mater 2003; 51(20): 6329-6340.

[25] Weidner A, Tirschler W, Blochwitz C. Overstraining effects on the crack-opening displacement of microstructurally short cracks. Mater Sci Eng A 2005; 390(1-2): 414-422.

[26] Hadianfard MJ, Mai YW. In situ SEM studies on the effects of particulate reinforcement on fatigue crack growth mechanism of aluminium-based metal-matrix composite. J Mater Sci 1995; 30(21): 5335-5346.

[27] Mutoh Y, Zhu SJ, Hansson T, Kurai S, Mizuhara Y. Effect of microstructure on fatigue crack growth in TiAl intermetallics at elevated temperature. Mater Sci Eng A 2002; 323(1-2): 62-69.

[28] Chan KS, Jones P, Wang Q. Fatigue crack growth and fracture paths in sand cast B319 and A356 aluminum alloys. Mater Sci Eng A 2003; 341(1-2): 18-34.

[29] Tokaji K, Kamakura M, Ishiizumi Y, Hasegawa N. Fatigue behavior and fracture mechanism of rolled AZ31 magnesium alloy. Int J Fatigue 2004; 26: 1217-1224.

[30] Gall K, Biallas G, Maiers HJ, Gullett P, Horstemeyer MF, McDowell DL, et al.. In situ observations of high cycle fatigue mechanisms in cast AM60B magnesium in vacuum and water vapor environments. Int J Fatigue 2004; 26: 59-70.

[31] Wang XS, Fan JH, Wu BS, Li Y. Effects of spacing and alignment pores on fatigue crack behaviors of cast magnesium alloys. Adv Fract & Mat Behavior 2008; 33-37:13-18.

[32] Wang RM, Eliezer A, Gutman EM. An investigation on the microstructure of an AM50 magnesium alloy. Mater Sci Eng A 2003; 355: 201-207.

[33] Horstemeyer MF, Yang N, Gall K, McDowell DL, Fan J, Gullett PM. Fat Fract Eng Mater Struct 2002; 25; 1045-1056.

[34] Padfield TV, Handbook of metallography and microstructures, vol. 9. Materials Park (OH): ASM; 2004.

[35] Lu YZ, Wang QD, Zeng XQ, Ding WJ, Zhao CQ, Zhu YP. Effects of rare earths on the microstructure, properties and fracture behavior of Mg-Al alloys. Mater Sci Eng A 2000; 278: 66-76.

[36] Moreno IP, Nandy TK, Jones JW et al. Microstructural characterization of a die-cast magnesium rare earth alloy. Scripta Mater 2001; 45: 1423-1429.

[37] Zheng WC, Li SS, Tang B, Zeng DB, Guo XT. Effect of rare earths on hot cracking resistant property of Mg-Al alloys. J Rare Earth 2006; 24(3): 346-351.

[38] Li SS, Zheng WC, Tang B, Zeng DB, Guo XT. Grain coarsening behavior of Mg-Al alloys with mischmetal addition. J Rare Earth 2007; 25(2): 227-232.

[39] He SM, Peng LM, Zeng XQ, Liu LP, Wang QD, Ding WJ, Zhu YP. Effects of variable La/ Ce ratio on microstructure and mechanical properties of Mg-5Al-0.3Mn-1RE alloys. Mater Sci Forum 2005; 488-489: 231-234.

[40] Paris PC, Erdogan F. A critical analysis of crack propagation laws. Trans ASME J Basic Eng 1963; 85: 528-534.

[41] ASTM: E647. Standard test method for measurement of fatigue crack growth rates. ASTM standards. The American Society for Testings and Materials 03.01 1998; p562-598.

[42] Ramberg W, Osgood WR. Description of stress-strain curves by three parameters. *National Advisory Committee for Aeronautics -- Technical Notes* 1943; p13.

[43] Wang XS, Kawagoishi N. Simple predicting method for fatigue crack growth rate based on tensile strength of carbon steel. J Iron & Steel Res Int 2003; 10(2): 58-62.

[44] Wang XS, Xu Y, Xu XQ. Direct observations of microcracking in the fuel plate using the scanning electron microscope. J App Comp Mater 2004; 11(3):145-154.

[45] Wang XS, Wu BS, Wang QY. Online SEM investigation of micro fracture characteristics of concretes at various temperature values, Cement Concrete Res 2005; 35(7): 1385-1390.

[46] Wang XS, Liang F, Zeng YP, Xie XS. SEM in-situ observations to investigate the effects of inclusions on the low cyclic fatigue crack initiation and propagation of super strength steel, Acta Metall Sin 2005; 41(12):1272-1276.

[47] Wang XS, Zhang LN, Zeng YP, Xie XS. SEM in-situ investigation on fatigue cracking behavior of P/ M Rene95 alloy with surface inclusions. J Uni Sci Tech Beijing-Mater 2006;13(3): 244-249.

[48] Wang XS, Yan CK, Li Y, Xu YB, Meng XK, Wu BS. SEM in-situ study on failure of nanocrystal metallic thin films and substrate structure under three point bending. Int J Fracture 2008; 151: 269-279.

[49] Rice JR, ASTM STP 1973; 536: 231-245.

[50] Wang XS, Xu Y. Experiments, characterizations and analysis of a dispersion U3Si2-Al fuel plate with sandwich structure. J Nucl Mater 2004; 328(2-3): 243-248.

[51] Kawagoishi N, Wang XS, Nisitani H, Goto M, Kondo E, Prediction of Fatigue Life Based on Small Crack Growth Law. Trans JPn Soc Mech Eng A 1997; 63(613): 1867-1873.

[52] Gutman EM, Eliezer A, Unigovski YE, Abramov E., Mechanoelectrochemical behavior and creep corrosion of magnesium alloys. Mater Sci Eng A 2001; 302: 63-67.
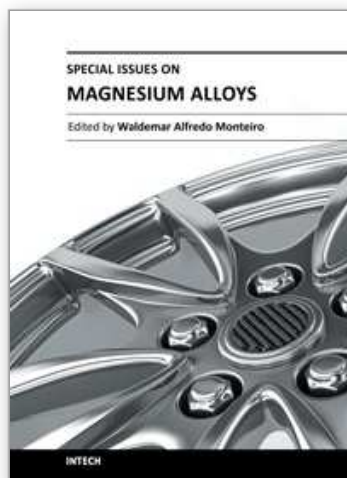
Special Issues on Magnesium Alloys

Edited by Dr. Waldemar Monteiro

Magnesium is the lightest of all the metals and the sixth most abundant on Earth. Magnesium is ductile and the most machinable of all the metals. Magnesium alloy developments have traditionally been driven by requirements for lightweight materials to operate under increasingly demanding conditions (magnesium alloy castings, wrought products, powder metallurgy components, office equipment, nuclear applications, flares, sacrificial anodes for the protection of other metals, flash photography and tools). The biggest potential market for magnesium alloys is in the automotive industry. In recent years new magnesium alloys have demonstrated a superior corrosion resistance for aerospace and specialty applications. Considering the information above, special issues on magnesium alloys are exposed in this book: casting technology; surface modification of some special Mg alloys; protective carbon coatings on magnesium alloys; fatigue cracking behaviors of cast magnesium alloys and also, magnesium alloys biocompatibility as degradable implant materials.

INTECH
open science | open minds